

To the Graduate Council:

I am submitting herewith a thesis written by Gerald Robert Callison entitled “An Evaluation of the Cascaded H-Bridge Multilevel Inverter Topology For Direct-Drive Synchronous Wind Farm Applications.” I have examined the final electronic copy of this thesis for form and content and recommend that it be accepted in partial fulfillment of the requirements for the degree of Master of Science, with a major in Electrical Engineering.

Leon M. Tolbert

---

Major Professor

We have read this thesis and  
recommend its acceptance:

Jack S. Lawler

---

Fangxing Li

Accepted for the Council:

Anne Mayhew

---

Vice Chancellor and  
Dean of Graduate Studies

(Original signatures are on file with official student records.)

**AN EVALUATION OF THE  
CASCADED H-BRIDGE  
MULTILEVEL INVERTER  
TOPOLOGY FOR DIRECT-DRIVE  
SYNCHRONOUS WIND FARM  
APPLICATIONS**

**A Thesis Presented for the Master of Science Degree in  
Electrical Engineering**

**Gerald Robert Callison  
May 2006**

*Dedicated to Charles, Susan, Leah, Katy, Annie, and Cindy Callison*

## **ACKNOWLEDGEMENTS**

I would like to extend my most sincere gratitude to Dr. Leon Tolbert, Dr. Jack Lawler, and Dr. Fangxing Li, who have not only served as members of my thesis committee, but have been instructors, mentors, and friends to me. I would also like to thank my classmates for answering questions, supporting me, and making the two years that I spent in graduate school a remarkable time in my life. Michael, Ben, Niranjana, Pankaj, Tim, Rui, Weston, Faisal, Steve, Chris, Pierre, Lakshmi, Surin, Zhong, Mengwei, Jeremy, Kaiyu, Wendy, Lucy, Saijun, Yan, Haiwen, Hui, SeongTaek, and Curtis. As I approach my time to move on, I find myself with much more than the degree I came to the University of Tennessee for. I find myself with lifelong friends. Finally, I would like to thank my high school technology education teacher, Mr. Scott Lukas, who first inspired the passion in me, along with countless other students, to become an engineer.

## **ABSTRACT**

A key driver in the recent success of wind has been engineering advances that have led to improved economics. Many of these advances have centered on power electronic converters, which feature a rectifier that converts the uncontrolled alternating current output of a wind generator to direct current, and an inverter, which converts that direct current back to a controlled alternating current synchronized with the power grid to which the wind generator is connected. Most of the inverters on today's market use the full-bridge topology, which features six power electronic switches per wind turbine. The purpose of this thesis is to investigate if the cascaded H-bridge multilevel inverter offers benefit in terms of improved economics. Potential advantages of the cascaded H-bridge inverter include reduced switch count, improved converter efficiency, and simplified interconnection to the utility. Potential drawbacks include an increase in required power electronic switch ratings and a reduced ability to withstand transient wind conditions. This thesis concludes that certain control schemes can address performance under transient wind (and thus power production) conditions and that improvements in converter efficiency and reduction in switch counts are offset by increased switch requirements. Therefore, any benefit to justify the use of the cascaded H-bridge inverter in wind farms will arise from a simplified point of common connection to the utility.

## TABLE OF CONTENTS

1	INTRODUCTION .....	1
1.1	Background On Wind Energy.....	2
1.2	Background on Power Conversion .....	8
2	LITERATURE REVIEW .....	13
2.1	Control Issues in Direct-drive Synchronous Wind Systems.....	13
2.2	Stability Impact of Wind Farms.....	14
2.3	Cascaded H-bridge Multi-level Inverters.....	18
2.4	Loss Modeling in IGBTs .....	26
3	SIMULATION.....	29
3.1	Assumptions.....	29
3.2	Assumed Properties of the IGBT .....	31
3.3	Top Level Dynamic Wind Cascaded H-Bridge Model.....	32
3.4	The Controller.....	33
3.5	The Rank Assignment Block .....	33
3.6	The Comparator Array .....	36
3.7	The Multiplexer Driver .....	36
3.8	H-bridge and IGBT .....	38
3.9	Utility Interface.....	44
3.10	Cascaded H-Bridge Inverter Model for Efficiency and Component Size .....	44
3.11	Full-Bridge Inverter Model.....	46
4	RESULTS .....	50
4.1	Determining Simulation Parameters .....	50
4.2	Full-Bridge Efficiency Simulations, A Baseline for Comparison .....	52
4.3	Cascaded H-Bridge Inverter Efficiency Calculations.....	53
4.4	Full-Bridge Simulations For Component Sizing .....	56
4.5	Cascaded H-bridge Simulations For Component Sizing .....	56
4.6	Cascaded H-bridge Simulations, Control Under Dynamic Wind.....	58
5	CONCLUSIONS/FUTURE WORK.....	65
5.1	Conclusions.....	65
5.2	Future Work .....	69
	BIBLIOGRAPHY.....	72
	Vita.....	75

## LIST OF TABLES

<b>Table</b>		<b>Page</b>
4.1	Results of simulations run with full-bridge inverter at various power levels.....	52
4.2	Breakdown of total power loss into conduction and switching losses.....	52
4.3	Results of the efficiency calculations, including output power without switching losses, input power from each H-bridge, total input power, switching energy from each H-bridge, total switching energy, power lost in switching, total output power, power lost to conduction, and overall converter efficiency.....	54
4.4	Breakdown of total power loss into switching and conduction losses.....	55
4.5	Comparison of losses in full-bridge and cascaded H-bridge inverters.....	55
4.6	Power production rankings for each SDCS over the duration of the simulation...	62
5.1	Power lost per switch in each converter.....	67

## LIST OF FIGURES

Figure	Page
1.1	Typical Coefficient of Performance versus Tip Speed Ratio relationship.....5
1.2	Standard topology of a direct-drive synchronous wind energy conversion system.....8
1.3	One phase of an $m$ level cascaded H-bridge multilevel inverter.....10
1.4	Line to neutral voltage of one of the phases of the cascaded H-bridge inverter, when using a standard, staircase-switching scheme.....10
2.1	The standard topology of an individual H-bridge.....22
2.2	Pulses evenly distributed between different levels to attain the desired line to neutral voltage.....24
3.1	Top-level model of the inverter, without the output line filters.....32
3.2	The controller block.....34
3.3	The rank assignment block.....35
3.4	Topology of the comparator array.....37
3.5	Multiplexer driver block.....39
3.6	The topology of the H-bridge block.....40
3.7	Model of the IGBT, including switching losses.....42
3.8	The model of the utility interface.....45
3.9	Cascaded H-bridge model with simplified control used for efficiency and component sizing studies.....47
3.10	The full-bridge model's topology.....48
4.1	Percentage of total switching losses per level. 5 represents the H-bridge at the top and bottom of the waveform, while 1 represents the H-bridge at the middle of the waveform.....54
4.2	Instantaneous collector currents (in Amps) experienced by all six switches during the operation of the full-bridge inverter at 750 kW commanded.....57
4.3	Instantaneous collector currents (in Amps) experienced by all six switches during the operation of the full-bridge inverter at 2,250 kW commanded.....57
4.4	The collector current (in Amps) for all switches in the H-bridge module closest to the middle of the output waveform, when each module is commanded to provide 2,250 kW.....59
4.5	The collector current (in Amps) for all switches in the H-bridge module closest to the outside of the output waveform, when it is commanded to provide 750 kW...59
4.6	The collector current (in Amps) for all switches in the H-bridge module closest to the middle of the output waveform, when each module is commanded to provide 2,250 kW.....60
4.7	The collector current (in Amps) for all switches in the H-bridge module closest to the outside of the output waveform, when each module is commanded to provide 2,250 kW.....60
4.8	Output voltages of each H-bridge module under static wind conditions.....61
4.9	Output voltages of each H-bridge under dynamic wind conditions.....63

## 1 INTRODUCTION

Wind energy is currently the fastest growing source of electric generation in the world, providing more than 31, 000 MW of power generation worldwide [1]. Advocates for wind energy maintain that it could provide 12 percent of all electric power generated in the world by the year 2020 [1]. For environmentalists concerned about pollution, policy makers concerned about reliance on fossil fuels, and investors hoping to profit from a new source of energy, the advancement of wind power holds wonderful promises. However, for power grid operators, the advancement of wind energy holds many challenges. Wind power is unsteady, unpredictable, and harnessed in relatively small quantities at points spread over a large area. If it is not properly controlled, the power output of a wind farm could rise by over 10 percent in just 2 seconds [1]. On top of all of this, the electricity that the generators put onto the grid must occur at the grid's frequency. Thus, wind farms cannot be tied directly to the power grid without devices to help regulate and control their output. However, the most technologically advantageous *wind energy conversion system* features a superb power electronic interface to the external power grid to which it is connected. This system, which is referred to as *direct drive synchronous*, features a synchronous generator whose AC output is immediately rectified to DC, and is then inverted back to an AC voltage that is compatible with the grid into which it is being fed. This system is highly advantageous because the inverter can control both the reactive power content and the frequency of the electricity being put onto the grid.

This thesis will compare two inverter topologies for conditioning the power from each wind turbine in a direct drive synchronous wind farm to the grid suitable AC. One inverter considered will be the standard used today, the full-bridge. The other system to be considered is the cascaded H-bridge multilevel, one that shows great promise. It will focus on component count and sizing considerations (and thus cost), performance of each inverter topology, and how well each topology is able to interface with the external power grid. While the standard variety of inverter, the three phase H-bridge, requires six power-electronics switches per wind turbine, the cascaded H-bridge multilevel inverter discussed in this thesis only requires four power-electronic switches per wind turbine. However, the switches in the cascaded H-bridge inverter will need to be rated for slightly higher current than those in the standard full-bridge inverter. Thus, it is hoped that the cascaded H-bridge inverter will demonstrate superior economic potential due to its lower switch count (not being out-weighted by the higher switch rating requirements) and the elimination of the transformer that would link a full-bridge inverter to the external power grid.

## **1.1 Background On Wind Energy**

Before discussing in depth solutions related to specific problems associated with wind generation, it is necessary that some background information be presented. Successful implementation of a wind energy conversion system requires expertise in a myriad of fields, from electrical engineering experts to meteorology experts to even ornithology experts that can study the impact that a wind farm at a specific location will

have on bird and bat mortalities. This discussion will focus on the wind energy concepts relevant to an electrical engineer.

Regardless of what type of wind energy conversion system is being used, there are some fundamental equations and properties that apply to all systems. The basic equation for electric power generated by an individual wind turbine is:

$$P = \frac{1}{2} \rho A v^3 C_p N_g N_b \quad (1.1)$$

where:

$P$  = electric power output from a specific wind generator

$V$  = wind velocity (meters/second)

$\rho$  = density of air at turbine blades

$A$  = area swept by the rotor blades

$C_p$  = coefficient of performance

$N_g$  = the efficiency of the generator machine

$N_b$  = the efficiency of the gearbox that steps the speed of the rotor blades to the speed of the generator

The coefficient of performance,  $C_p$ , is a very important quantity, which represents the efficiency of the blades in capturing energy from the surrounding moving air. Every design of turbine blades has a unique coefficient of performance curve, which varies relative to the ratio of the linear speed of the blade tips to the surrounding wind

(this is called the *tip-speed ratio*, or *TSR*). A typical  $C_p$  vs. TSR curve appears as follows in Figure 1.1.

For each of these curves, there is a specific TSR for which the coefficient of performance reaches a maximum value, and thus it is a goal of many wind turbine controllers to control the rotor speed such that the maximum coefficient of performance is attained.

There are three main types of systems for generating wind energy. Although this thesis will focus on only one system, the direct-drive synchronous system, a discussion of all systems will be briefly presented at this point:

- Squirrel-cage induction
- Doubly fed induction
- Direct-drive synchronous

The *squirrel-cage induction system* represents the oldest system. It consists of a squirrel cage induction machine that feeds the electricity it generates directly onto the power grid. Capacitor banks and/or Flexible AC Transmission System (FACTS) devices are connected to the output terminals of the generator in order to condition the power as it is put onto the grid. Specifically, they are necessary because squirrel-cage induction generators consume large amounts of reactive power and are incapable of generating their own. Because the mechanical rotor speed is directly coupled to the electrical frequency of the generator's output power and the external power grid, the turbine must rotate at a constant speed in this system. Control over this rotating speed is accomplished through the use of aerodynamic devices, such as variable pitch rotor blades (this is the case in most systems, not just squirrel cage induction based systems). The fixed speed and direct

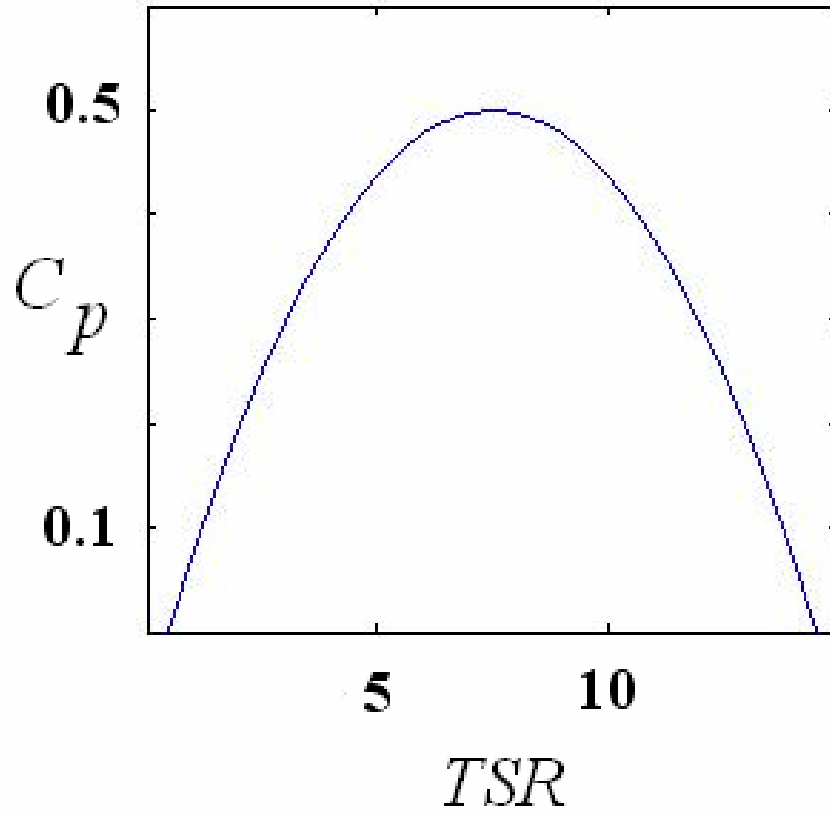


**Figure 1.1** Typical Coefficient of Performance versus Tip Speed Ratio relationship

coupling to the power grid lead to a high level of inflexibility that is a tremendous disadvantage to this system [2].

The next system is the *doubly fed (or wound rotor) induction system*. Like the squirrel cage induction generator, this system features an induction machine tied directly to the power grid (and also requires reactive power compensation). However, this machine features rotor windings that can be electrically accessed and fed from an external voltage source or run through a variable resistance. They are accessed from the outside by slip rings on the rotor, much like a non-permanent magnet synchronous machine. Thus, the electrical rotor frequency can be controlled independently of the mechanical rotor speed, and variable speed operation of the rotor is allowed [2]. This also provides an opportunity to control the speed of the wind turbine and output power of the generator [4]. However, this machine is relatively inefficient (its efficiency percentage is usually in the mid eighties) because some output power must be fed back into the rotor. Additionally, doubly fed induction machines are rarely used in applications other than wind, so they cannot take advantage of the economies of scale to the extent that generators for the other two systems can. Still, due to the fact that this system provides variable speed operation with smaller power electronics requirements than the synchronous system, and since the synchronous system's adoption has been hindered in the North American market by patent restrictions, the doubly fed system is the most common system in use today.

The final major system is the *direct drive synchronous system*. It features a synchronous machine that is excited using either an external source or permanent magnets. Rather than having the generator outputs tied directly to the grid, it is tied to a

power electronic based converter. The converter usually features a rectifier that outputs power onto a DC link that feeds an inverter. The DC link voltage can be controlled either through a controlled rectifier or with a DC to DC converter added between the rectifier and inverter [3]. Synchronous generators cannot be tied directly to the grid due to their need to be synchronized before connecting and their volatile performance under a varying prime mover.

However, connecting through a power converter offers a number of advantages, which make this system the most desirable to date (cost and patent issues notwithstanding). And with the power converter's ability to decouple the generator's output from the grid, synchronous generators, which are smaller, lighter, and cheaper than induction generators (in the case of those whose rotors are slip-ring fed), can be used in this case. Although permanent magnet generators are used in small, residential sized systems, externally slip-ring fed generators are commonly used in utility scale systems (although *General Electric* has recently introduced mid-range utility scale models with permanent magnets). The converter gives the system enough flexibility for variable mechanical rotor speed and, at least theoretically, can provide reactive power for voltage support [2]. Another major advantage of this system is that the rectifier can exert control electrically over the generator to command a specific torque, and thus rotational speed. Such a system was proposed in [3], which included a passive rectifier used with a DC to DC converter, to reduce the amount of active switches required. Yet another advantage to this system is that, if a generator with a sufficiently high pole count is used, the rotor blades can turn the generator directly, without the gearbox that is required in the other two systems.

## 1.2 Background on Power Conversion

The full-bridge single level inverter is the topology most commonly used in systems today. It features a rectifier that feeds a DC link that supplies a full-bridge pulse-width modulated inverter, which is located at each turbine. The system is shown in Figure 1.2.

In this system, one complete inverter exists for each wind turbine. Each inverter produces a three phase AC that is synchronized to the surrounding power grid, and then fed to it through a transformer. This system requires a transformer to step up the voltage of the power converter before the power is injected into the grid. This system is ideal for wind farms with a very small amount of wind turbines. While there are a number of wind farms with as few as one turbine, there are also a number of large wind farms that have hundreds of turbines.

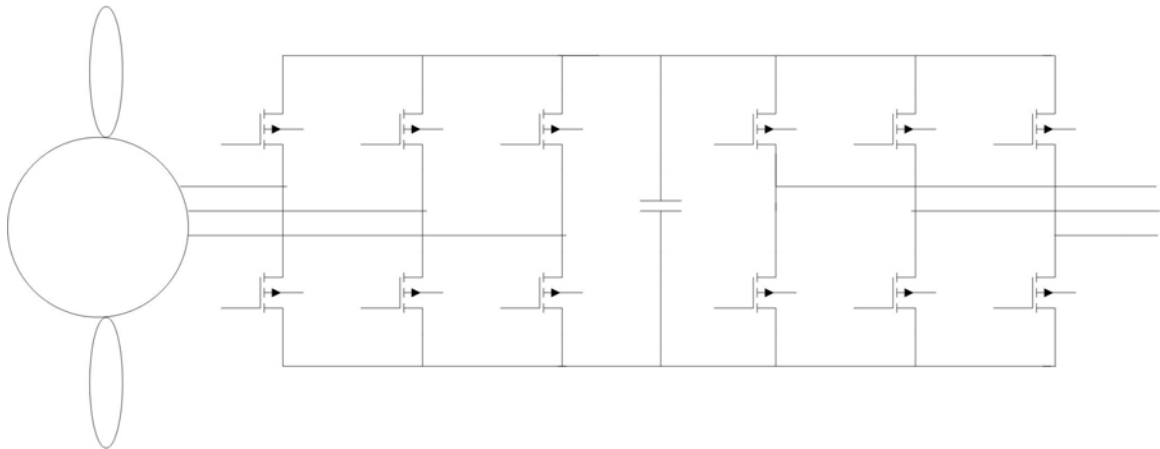


**Figure 1.2** Standard topology of a direct-drive synchronous wind energy conversion system [3]

For wind farms with larger numbers of turbines, it is possible that another inverter topology could work. On paper, the cascaded H-bridge multilevel inverter topology shows great potential for application in large wind farms. Multilevel inverters in general are desirable for utility applications because they have low harmonic outputs and can interface to high-voltage power grids with greatly simplified filtering requirements and without the use of transformers (depending upon the application). They are so good in this regard that they have been the enabling technology for a number of utility scale applications of power electronics.

The cascaded H-bridge multilevel inverter consists of a series of single-phase H-bridge inverters whose outputs are connected to each other, and whose inputs each come from a different *Separate DC Source*, or *SDCS*. The cascaded H-bridge multilevel inverter's topology and line to neutral voltage output of one of the phases is shown in Figures 1.3 and 1.4.

From the output scheme shown in Figure 1.4, one can understand some of the control challenges faced in the use of the cascaded H-bridge inverter. When comparing the time that P5 is on to the time that P1 is on, it becomes apparent that the power drain requirements vary from voltage level to voltage level. Therefore, different separate DC sources must be used for different levels at different times, being coordinated in such a way that the power requirements from each source are evened out. This would not be difficult to do were each separate DC source completely identical in terms of voltage and power generation. However, this is certainly not the case when each separate DC source represents a unique wind turbine, which is located in a unique spot, and subjected to unique wind conditions! Therefore, the control scheme must take into account the power

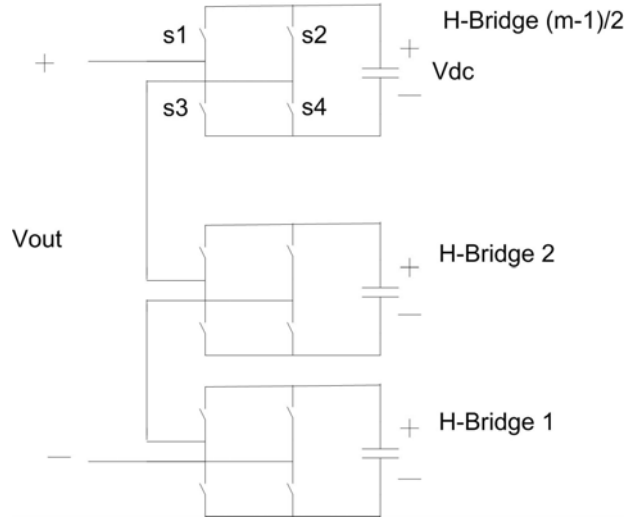


**Figure 1.3** One phase of an  $m$  level cascaded H-bridge multilevel inverter

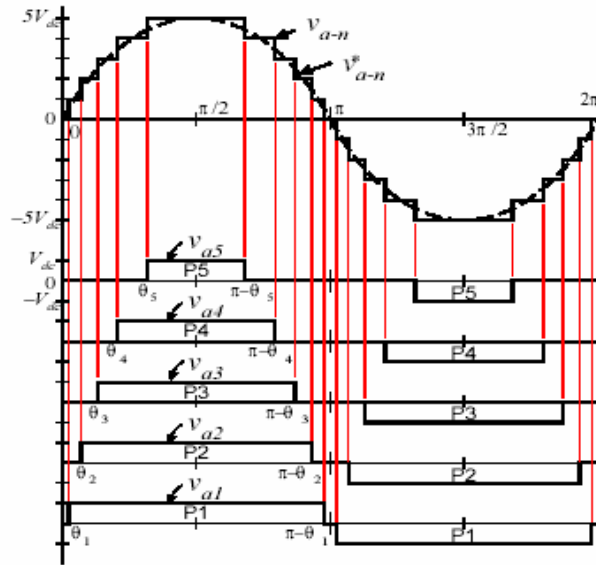


**Figure 1.4** Line to neutral voltage of one of the phases of the cascaded H-bridge inverter, when using a standard, staircase-switching scheme [8]

being generated by each turbine (or SDCS) when assigning a turbine to a voltage level [8]. This can involve taking more power out of a turbine that is generating higher power levels, so it is important to note that the goal in control is *appropriate* power drain from each SDCS, not *equal* power drain from each SDCS.

It should also be noted that the Cascaded H-bridge Inverter has a significant capability that will not be explored in this thesis. Having a greater number of voltage levels is highly advantageous, because doing so results in lower harmonic content, and thus in lower filtering requirements. A Cascaded H-bridge with  $s$  number of separate DC sources that all have an equal voltage magnitude can attain as many as  $2s+1$  voltage levels. However, by assigning voltage magnitudes to each source that increase by a factor of 2 (Vdc, 2Vdc, 4Vdc, 8Vdc, ...), the number of voltage levels that can be attained by the output increases dramatically. Consider such an inverter with 3 SDCSs, at 10 volts, 20 volts, and 40 volts. Such an inverter could attain voltage levels as high as the sum of all SDCSs (+/-70 volts in this case), along with any value in between by increments of its smallest SDCS (10 volts, in this case). Controlling such an inverter to attain proper power drain between SDCSs becomes incredibly difficult, especially in the situation of this thesis where each SDCS represents a specific wind turbine.

Additionally, this control scheme would involve more frequent switching, since each H-bridge needs to coordinate with each other to form a certain level, and therefore would most likely have to switch values many times through a given line cycle (versus the method used with equal SDCSs, in which each H-bridge assumes only one value during each maximum or minimum in the cycle). Thus, consideration of different voltage levels

among SDCSs will be out of the scope of this thesis, so this thesis will study only a situation in which SDCSs have equal voltage levels [8].

Although wind energy holds a great deal of promise, it also holds a great deal of challenges. One significant challenge faced in its advancement is to maximize the performance of inverters for the direct-drive synchronous system while minimizing their cost. The purpose of this thesis is to evaluate if the cascaded H-bridge multilevel inverter topology has the ability to accomplish that goal.

The next chapter of this thesis will present a survey of current literature related to wind farms. From the stability of power systems under changing wind conditions to different methods for modulating cascaded H-bridge inverters, there is a variety of issues that need to be evaluated in order to gain an accurate perspective on how this thesis relates to current direct-drive synchronous wind farm research.

## **2 LITERATURE REVIEW**

Although no specific literature exists on the use of the cascaded H-bridge inverter for wind farms, some literature exists covering cascaded H-bridge inverters, and a great deal of literature exists for direct-drive synchronous wind farms. An examination of literature in these areas related to this thesis will be conducted in this chapter.

### **2.1 Control Issues in Direct-drive Synchronous Wind Systems**

A discussion of the control of a direct drive synchronous system occurred in a paper entitled, "Implementation of Grid Connected AC-DC-AC Power Converter for Variable Speed Wind Energy Conversion System." The inner workings of an AC-DC-AC power converter for the direct drive synchronous WECS is presented in this paper. With a discussion of a proposed control system and experimental results, the authors show how the system is able to exercise precise control over parameters such as voltage output, real and reactive power output, and commanded generator torque under the dynamic conditions that a wind generation system faces [3].

The overall AC-DC-AC converter can be subdivided into three individual converters: an uncontrolled 3-phase diode rectifier, a boost DC to DC converter, and a full-bridge Pulse Width Modulation (PWM) 3-phase inverter. In addition to the power converters themselves, there were various controllers and sensors throughout the system. Because the rectifier was uncontrolled, its output voltage was proportional to the speed of the wind rotors, so that voltage was used to calculate the rotor speed. The boost converter, which featured a single Insulated Gate Bipolar Transistor (IGBT), was

controlled in such a manner to insure that the torque commanded from the power converter matched the torque produced by the rotors subjected to the wind so that the rotors would not speed up uncontrollably. The boost converter was used rather than a controlled rectifier in order to reduce the semiconductor switch count, and thus the cost, of the system. The PWM inverter is controlled through a proportional integral based scheme that takes its commanded values from a q-d reference frame. Q axis current controls active power whereas D axis current controls reactive power [3].

This proposed system was then tested, using a 30 kW wind turbine. The results first showed how the system responded to a change in the commanded current from the rectifier (which would have the effect of changing commanded torque on the generator). Although there was a relatively slow response time for the actual current, of 0.2 seconds, this is acceptable since the dynamics of wind are relatively slow as well. A number of other satisfactory results were shown, including successful regulation of the inverter's output voltage when the input voltage to the rectifier varied from 140 to 250 volts [3].

## **2.2 Stability Impact of Wind Farms**

An important consideration in the study of interconnecting power generation to the power grid is the impact that it will have on stability of the system. This represents a key area that needs further research, because the vast majority of studies that consider the impact of wind energy on power system stability do so for wind systems using the squirrel cage induction or doubly-fed induction systems. Although small wind farms do not represent a significant factor in power system stability, large ones present a tremendous factor, and since the cascaded H-bridge topology is well suited for larger

wind farms, stability impact is an issue that must be explored. Therefore, a brief look at stability in the face of transient wind conditions, even with an asynchronous wind farm, is worthwhile.

A miniature power system, with an asynchronous wind generator, was set up in [10] to study the impact that varying wind conditions had on the overall power system. The system used was designed to be a smaller, scaled down version of a typical national power grid. It consisted of two synchronous generators, SG1 and SG2, which are 75 MVA and 35.3 MVA respectively, and AG3, which represents the wind farm. Along with the three generators, the mini-grid contained eight busses, three loads, two transformers, and two capacitors for voltage support (in addition to two capacitors used to represent the reactive power output of the two synchronous generators). It is common practice in utilities to limit the amount of wind power connected into a power grid at a specific point to 7 % of that point's short circuit power. The short circuit power in this case was calculated to be 132 MVA, so 7 % of that would be 9.24 MVA. To test this limit (along with the overall stability impact of wind), two arrangements of the wind farm were used: one consisting of twenty-five 1 MW (nominal capacity) machines and one that had only ten 1 MW machines. Both of these generators featured automatic generation control to regulate both their voltage and speed (as most power plants do). It should be noted that 25 MW represents 19 % of the short circuit power, nearly three times the limit that is used in common practice [10].

The models both with 25 MW and 10 MW of wind were then built with an in-house MATLAB based program, that uses the Runge-Kutta method to solve the system, and subjected to a variety of wind conditions. One simulation was designed to represent

turbulent wind (a rapid series of increases and decreases of speed), with wind transitioning from a steady state speed of 15 m/s to a high of 16.5 m/s and low of 9.5 m/s, with the turbulence lasting 14 seconds. The voltages of busses 1-5 were monitored, and in the case of the 25 MW of wind generation, all fluctuations were less than 2 %, and in the case of 10 MW of wind, all fluctuations were within 1 %. Frequencies stayed within 0.14 Hz and 0.065 Hz of nominal value for the 25 turbine and 10 turbine cases, respectively. Next, simulations were run to simulate wind gusts (three rapid wind speed spikes representing 25 % increases, but no decreases). When subjected to these conditions, the bus voltage in the load bus (bus 5) varied by just 0.215 %. Such extremely small variation can be attributed to the fact that the gusts were of extremely small time duration, so their effects were largely dampened by the inertia of the wind turbines. Frequency stayed within 0.035 Hz of its nominal value. The final test that the system was subjected to was the disconnect of the entire 25 turbine wind farm (which would have a more significant impact than the disconnection of the 10 turbine wind farm), which is a legitimate concern since wind farms are often disconnected when problems occur on the power grid or with bad weather. Results showed that when the wind farm was disconnected, non-wind generator SG1's active power output had an overshoot of about 11 %, and non-wind generator SG2's active power had an overshoot of about 10 %, while their responses both settled to a new steady state within about 6 seconds. System frequency variation was between -0.46 and 0.1 Hz, while all bus voltages immediately rose and then decreased to lower levels than they were at before the disconnection. The voltage and frequency responses to this simulation were all considered to be acceptable. All of the results of the tests performed in this paper

indicated that adding wind generation of 19 % of short circuit power to a single point in the power grid will not adversely affect voltage, frequency, or active power response that would cause instability of the system [10].

The authors of paper [12] performed a study of power system stability with a direct-drive synchronous wind farm. Stability of the power system becomes significantly simpler when a direct-drive synchronous wind farm is used. This is because the power converter can provide reactive power voltage support and isolate the power grid from most of the electrodynamic of the machine, and thus the power grid only sees the power converter (a Current-Controlled Voltage Source Inverter, in this paper) and its outputs, not the generator. For instance, the internal fluxes of the generator have no effect on the currents fed into the grid during a fault. In the study performed in [12], a 13-bus system was examined (which represented a fairly weak grid), with a 1.053 per unit volt slack bus and a single PQ bus representing the wind farm (where both real and reactive powers are specified). Harmonics are ignored (it is assumed that the PWM inverter is properly filtered), so the standard power flow equations can be used. A mechanical model of a permanent magnet generator based wind turbine was developed for this simulation, from which the electrical power output curve resulting from a specified turbulent wind curve was computed. The resulting power curve was then fed into a mathematical model of the power converter whose output was fed into a mathematical model (based on the standard power-flow equations) of the 13-bus network. A variety of simulations were then run to compute the voltages at all 13 busses, with the wind farm disconnected, the wind farm connected and inverters running at unity power factor, and the wind farm connected and inverter providing reactive power generation and absorption to mitigate voltage

fluctuations. It was discovered that while significant voltage fluctuations occurred during the unity power factor simulations (since this network model was meant to represent a relatively weak distribution network), they were reduced to acceptable levels when the inverter performed reactive power regulation [12].

### **2.3 Cascaded H-bridge Multi-level Inverters**

Although virtually no literature exists that studies the cascaded H-bridge inverter's performance in wind systems, literature does exist that studies the inverter's performance in FACTS applications. It is important to examine this literature not only for general cascaded H-bridge concepts, but also for certain FACTS considerations because, like a STATCOM, the cascaded H-bridge based wind farm must be able to supply reactive power for voltage support.

Research performed at Oak Ridge National Laboratory has focused on the use of this inverter in static var compensators. In paper [9], it is pointed out that the problem of unequal demand on SDCSs is not present in var compensation, because the current is shifted by  $\pm 90$  degrees relative to the voltage. Thus, the only discharge of the capacitors over a cycle is because of losses in the inverter. However, the paper pointed out that unequal demand on SDCSs is an issue if the inverter is used for harmonic filtering (and, although not mentioned in the paper, also if the inverter is being used for a wind farm). The authors of paper [9] proposed a control scheme in which only one of the capacitor's voltage is monitored, and based upon that, the duty cycle of each individual H-bridge is determined. This would work in a filtering type application because the

harmonics are spread evenly between phases and periodic. However, wind energy is completely random, so this system would require feedback from each SDCS (turbine) when applied to a wind farm.

The authors of paper [9] go on to discuss DC capacitor sizing issues for a shunt power line conditioner that provides reactive power support. It points out that all DC capacitors must have an equal value, since each SDCS must be able to be used for each voltage level (a consideration that holds true when the inverter is being used for a wind farm, as well). It also points out that harmonic currents have minimal impact on capacitor charge because of their high frequencies (so DC capacitor size requirements and output filter requirements will not affect each other). The main issue that affects capacitor sizing is the reactive output currents used for voltage support. The following equation is proposed to dictate DC capacitor size:

$$C_{dc} = \frac{\int_{\theta_1}^{T/4} \sqrt{2} I_{Cq} \cos(\omega t) dt}{\Delta V_{dc}} \quad (2.1)$$

$I_{Cq}$  represents the reactive current required for voltage support and  $\theta_1$  represents the angle from the beginning of the cycle to the point at which the lowest voltage level H-bridge turns on. The capacitance required for the cascaded H-bridge will be significantly higher than that for the traditional, two level inverter [9].

Issues related to the use of a cascaded H-bridge inverter as a STATCOM are also discussed in [15]. It points out the advantage that the cascaded H-bridge has over other multilevel inverter topologies, such as diode-clamped and flying-capacitor, include a

simple topology, modularity, and the ability to control each H-bridge separately from one another. Disadvantages include unequal current drains and voltage unbalance, which can make the output of the STATCOM difficult to control. In STATCOM operation, it is the magnitude of the converter output voltage that determines the direction of reactive power flow (a STATCOM is used to provide reactive power for voltage support) [15].

The authors of paper [15] then go on to discuss switching strategies, particularly emphasizing Fundamental Frequency Switching (FFS). FFS is a staircase-based switching scheme, in which the firing angles of each level are manipulated to selectively eliminate certain harmonics. The Fourier expansion of the  $n$ th harmonic of an  $m$  level stepped waveform is as follows:

$$V(n) = \frac{4V_{dc}}{\pi n} [\cos(n\alpha_1) + \cos(n\alpha_2) + \cos(n\alpha_3) + \dots \cos(n\alpha_m)] \quad (2.2)$$

where:

$\alpha_m$  is the switching angle of the  $m$ th voltage level and must be less than 90 degrees.

By solving the above equation, the switching angles can be determined that will eliminate certain harmonics. Methods of solving these equations for harmonic elimination is a subject of ongoing research, and although [15] proposed the use of the Newton-Raphson method, other papers, such as [16], have proposed methods based upon resultant theory. The switching patterns of each H-bridge are rotated every half cycle to achieve proper voltage balance between the SDCSs [15]. It should be noted that, in the wind farm application of the cascaded H-bridge, the power generation of each SDCS would need to be considered when assigning rotations between SDCSs. In experimental verification, the harmonics that were selected for elimination were not eliminated

completely because of voltage ripples in the SDCSs (capacitors, in this case). Still, the paper presented results that showed that an FFS switched cascaded H-bridge could perform suitably for a STATCOM application [15].

In paper [5], a variety of switching schemes were proposed for cascaded H-bridge inverters. A number of the switching schemes are designed to eliminate certain harmonics. Switching schemes were presented that can eliminate the 5<sup>th</sup>, 7<sup>th</sup>, and 11<sup>th</sup> harmonics while producing voltage at the commanded fundamental frequency with less total harmonic distortion than the standard staircase scheme shown in chapter 1. This is accomplished by selecting the switching angles using a look-up method based upon elimination theory [5]. This ability to selectively eliminate harmonics, using the switching schemes below, demonstrates the power of the cascaded H-bridge inverter.

Still other methods for switching exist. One method is a space vector PWM proposed in [11] (in this paper, all separate DC sources are equal). A primary advantage of this space vector PWM is that it offers possible mitigation when certain switches fail. To understand this at a fundamental level, one must consider the standard topology of a single H-bridge as shown in Figure 2.1.

By examining this topology, some inherent redundancies become apparent. In order to obtain a voltage of zero and bypass the H-bridge module, either switches T1 together with T3 or T2 together with T4 can be turned off. This means that, should either or both of the switches in the T1/T3 or T2/T4 combinations fail, the controller of the inverter can immediately adapt to the loss without discontinuing operation by simply

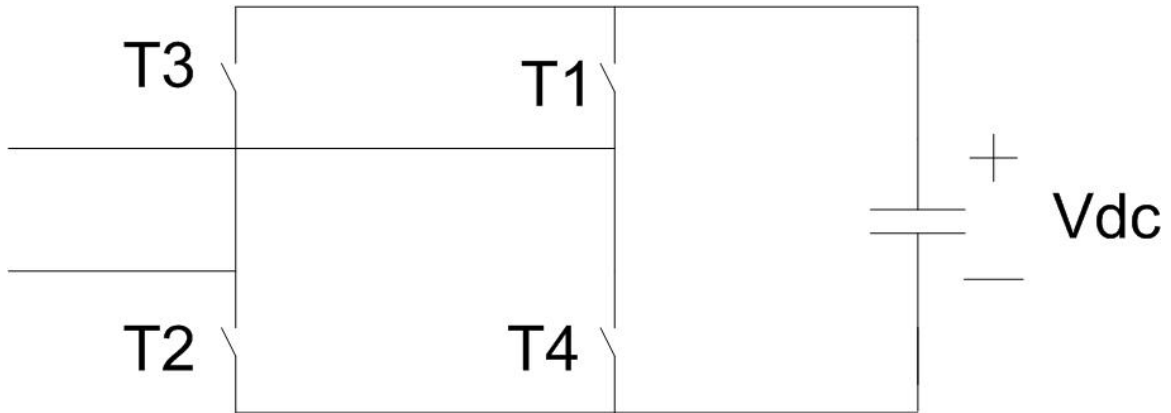


**Figure 2.1** The standard topology of an individual H-bridge

bypassing the H-bridge modules with failed switches. Still, the magnitude of the highest and lowest voltage levels attainable would each decrease by the product of the number of inactive H-bridges in each level times the voltage of the SDCS. For example, an inverter with three 1 volt SDCSs per phase could attain +/- 3 volts with all SDCSs working, while it would only be able to attain +/-2 volts if one phase had to be bypassed. One very crucial observation occurred in [11], and can be seen in the space vector diagram below, which represents a three-level inverter with all three levels on one phase shorted out.

Even with all SDCSs in one phase shorted out, there are still valid switching vectors. This is because, with the other phases working, the inverter is still able to manipulate voltage with respect to each line, and thus produce a balanced three phase line to line voltage. However, the inverter will not be able to produce as high of a voltage magnitude, and its phase voltages will be unbalanced [11].

A fully carrier based PWM method is proposed in [14] (which also works in a diode-clamped inverter), which is intended to improve switch utilization and balances the utilization of SDCSs. This method is similar to standard full-bridge PWM, and includes a single reference wave being compared to  $n-1$  triangular carrier waves ( $n$  is the number of levels), where the reference corresponding to zero is placed in the middle of the set of carrier waves. It is proposed for operation in low modulation indices. Low modulation indices occur at partial loading conditions of the inverter, and the problem is that in previous carrier based PWM methods not all levels are used when the amplitude of the reference signal is sufficiently small with respect to the carrier triangle signals (which is, by definition, what occurs at a low amplitude modulation index). This paper's authors propose a method of obtaining a more even usage of switches and SDCSs by taking advantage of redundant switching states to rotate usage among different levels at lower modulation indices. This method is especially advantageous to a cascaded H-bridge inverter, since they have both line to line redundancies and phase redundancies. Phase redundancies are exploited for the cascaded H-bridge, since this allows for each phase to operate independently of one another. The actual PWM method involves a standard look-up table, which takes input from the motor controller and modulation index calculator, and then outputs the gate signals into a pulse swapping circuit, which rotates the gate signals between different levels. Figure 2.2 shows how pulses are spread out between different levels to add up to the appropriate total line-neutral voltage. Note how the signals are evenly spread between levels, and how each level sees a smaller

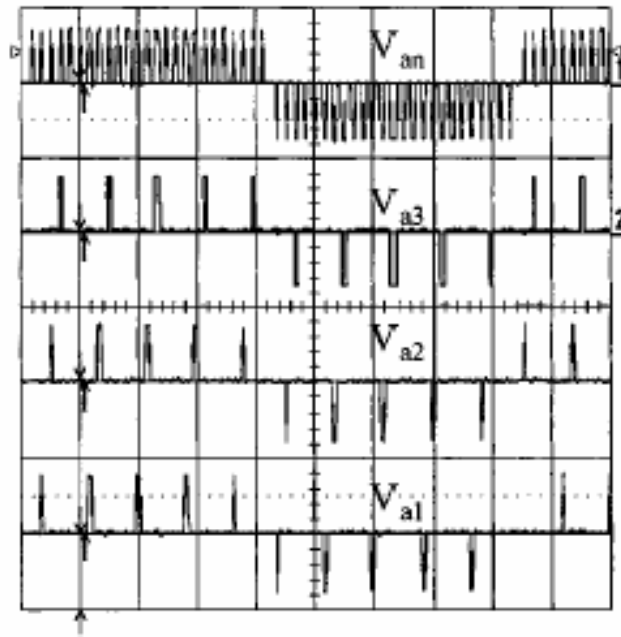


**Figure 2.2** Pulses evenly distributed between different levels to attain the desired line to neutral voltage [14]

switching frequency than that of the line to neutral output (which offers advantages of improved efficiency and decreased thermal stress) [14]. This proposed pulse-swapping method of PWM was experimentally verified using an 11 level, Y-connected MOSFET based inverter [14].

The authors of paper [13] present a look at a modified cascaded H-bridge inverter which is a hybrid in many regards, as it uses both Gate Turn Off Thyristors (GTOs) and IGBTs, and used a modulation scheme with step-type scheme in some cells and PWM in others. It should be noted that the voltages of each SDCS at each level are different. When using different SDCS values, significantly more levels can be attained than with equal SDCSs. For example, in a three H-bridge per phase inverter with 10, 20, and 60 volt SDCSs, the inverter has a range from  $-90$  to  $+90$  volts, and can attain any 10-volt increment between those two values.

The GTO H-bridge modules are switched using a step-type scheme, while the IGBT H-bridge modules are switched using PWM. The IGBT/PWM cells are assigned the lowest voltage SDCS, so that the harmonics generated from the PWM are of a lesser magnitude. The outputs shown in figure two of paper [13] demonstrate how this method can produce a very high quality output while minimizing switching for most of the higher voltage modules. The paper went on to point out the potential for loss of the ability to use full PWM, thus forcing the inverter to rely on the simple, staircase-switching scheme in order to attain certain output voltages. Consider what would happen if the largest SDCS in the inverter tested here was equal to 70 volts, as opposed to 60 volts. Although all 10 volt increment voltage levels could be attained from 10, 20, and 70 volt SDCSs for

a total of 21 levels, as opposed to just 19 levels from the 10, 20, and 60 volt SDCSs, the ability to use PWM on the 10 volt level is lost in the 10, 20, 70 configuration. This is because in certain configurations, the levels are reaching as far as they can. For example, in the 10, 20, 70 configuration, the inverter must reach as far as it can to attain +/-40 volts. What “reaching as far as it can” means is that the 10-volt SDCS must always be positive (for -40 volts) or always be negative (for +40 volts). This varies from the case of the 10, 20, 60 volt configuration where to attain +40 volts, for example, the sources would be +60 volts, -20 volts, and then the 10 volt source would modulate at both positive and negative levels in order to produce a waveform which more closely resembles a sine wave. And any PWM occurrence in any module will lessen the magnitude of its contribution. Therefore, if the 10-volt source must always be at its highest magnitude in order to reach a certain output, and PWM was applied to it, the inverter would not be able reach the desired output voltage magnitude. The paper went on to present satisfactory simulation results from an inverter with 100, 200, and 600 volt SDCSs [13].

## **2.4 Loss Modeling in IGBTs**

In order to evaluate the performance of the power electronic converters examined in this thesis, proper methods will be needed to evaluate the power losses in Insulated Gate Bipolar Transistors (IGBTs), the switches that will be used. Although the authors of paper [17] dealt specifically with power loss modeling in Silicon Carbide (SiC) MOSFETs, they presented some concepts that are relevant to an evaluation of IGBT

performance in full-bridge pulse-width modulated (PWM) inverters. The analysis presented here will focus on those areas that are relevant to IGBT loss modeling.

While the modeling of switching losses presented was more specific to MOSFETs, the modeling of conduction losses (in both the IGBT and the bypass diode) can be applied to IGBTs operating in a full-bridge PWM inverter. The paper first presents the following equation for conduction losses [17]:

$$P_{cond,Q1} = I_{Q1,rms}^2 * R_{DS,on} \quad (2.3) [17]$$

It then goes on to derive the following estimation for  $I_{Q1,rms}$  :

$$I_{Q1,rms} = I \sqrt{\frac{1}{8} + \frac{1}{3\pi} M \cos \phi} \quad (2.4) [17]$$

It then substitutes that estimation into the original equation for conduction losses, to create the following equation, which involves parameters that are all easily known:

$$P_{cond,Q1} = I^2 R_{DS,on} * \left( \frac{1}{8} + \frac{1}{3\pi} M \cos \phi \right) \quad (2.5) [17]$$

Where:

$R_{DS,on}$  = on resistance of the IGBT

$I$  = peak current through IGBT

$M$  = amplitude modulation index

$\phi$  = current phase angle (in radians)

The authors then go on to evaluate conduction losses in the bypass diodes. It points out that the equation for diode conduction losses is similar to that for IGBT losses, aside from the different duty cycles (since the bypass diode is on when ever the IGBT is

off, and vice versa). Thus, the following equation was presented to represent conduction losses in the bypass diode [17]:

$$P_{cond,D4} = I^2 R_D \left( \frac{1}{8} - \frac{1}{3\pi} M \cos \phi \right) + IV_D \left( \frac{1}{2\pi} - \frac{1}{8} M \cos \phi \right) \quad (2.6) [17]$$

The paper then went on to use the models described above, along with switching loss models (which are not relevant to a study of IGBT losses) to present an evaluation that showed favorable results for the use of SiC devices in a hybrid electric vehicle traction drive [17].

Current literature has examined a variety of issues related to this thesis. From the stability impact of changing wind conditions to different modulation strategies for cascaded H-bridge inverters, a number of different issues relevant to wind farms have been evaluated in this section. The next chapter will cover the simulation. It will discuss the design of the model, including the equations that were used and the assumptions that were made.

### **3 SIMULATION**

Three inverter models were created in Psim. One model represented one phase of a cascaded H-bridge multilevel inverter, with five separate DC sources (SDCSs) representing five wind turbines. This model also included control functions that were unique to the needs a wind farm, in which the power outputs of each SDCS had to be taken into account. Another model of the cascaded H-bridge inverter was created, with less control functions, to be used in simulations for determining efficiency and component sizing considerations. The third model represented a full-bridge inverter that would interconnect one wind turbine to the external power grid. Each model also contained components that represented an external power grid to which the inverter was connected.

#### **3.1 Assumptions**

Although some components that would exist in a real wind farm were ignored, approximated, or assumed to be ideal, the models that were created allowed for an in-depth evaluation of the H-bridge's performance and an in depth view of the full-bridge, which would serve as a baseline to compare with the H-bridge. Before evaluating the model itself, the assumptions that were made should be stated.

The first major assumption was related to the representation of each wind turbine. An actual wind farm built on this H-bridge topology would consist of a synchronous generator whose output voltage would depend on the wind speed. This varying AC voltage would then be rectified to the DC voltage required for each SDCS (which was

assumed to be done using a passive rectifier paired with a DC to DC converter, as opposed to an active rectifier). Once the desired SDCS voltage was attained, the output of each turbine would be fed into its own H-bridge level in the inverter, which would inject power into the external power grid. At this point of common connection to the grid, a filter would exist to reduce the harmonic output of the inverter (which would be low compared with a standard, full-bridge inverter). In the model used in this thesis, two different components were used to represent two different portions of each wind turbine. An ideal DC voltage source was used to represent the power output of each turbine, once the output had been conditioned to the prescribed SDCS level. Another DC voltage source was used to represent an analog reading of the output voltage on the DC link capacitor of each synchronous wind generator. The voltage level of the DC link capacitor is a key parameter needed in the control of the cascaded H-bridge inverter. As a wind generator creates power, it is either fed to the utility through the inverter or stored in the DC link capacitor, which is located between the wind generator and the DC to DC converter that adjusts the voltage for the inverter. As the level of power stored in the capacitor increases, so will the voltage across it, just as a decrease in the stored energy will cause the capacitor's voltage to decrease. Therefore, an analog signal representing the voltage on these capacitors (and thus power stored) is used to determine which level in the multi-level inverter each turbine will be assigned to.

Another major approximation was that only one phase of the 3-phase H-bridge was modeled and evaluated. This assumption was made because modeling all 3 phases would have created significantly more computing complexity and results to be evaluated, without yielding significantly more information. Because a basic, sine-triangle pulse-

width-modulation (PWM) was used, the overall performance can be accurately and more simply portrayed using a single phase. It should be noted that if this model was to include advanced fault recovery methods, such as the space-vector method outlined in [11], all 3 phases would need to be modeled, since line-to-line redundancies are used.

### 3.2 Assumed Properties of the IGBT

In order to perform this evaluation in a realistic manner, an IGBT model was created, with properties assigned to it that were typical of IGBTs in general. Some properties, such as power, current, and voltage maximums, had no relevance to the simulations that were run, since it was simply assumed that these limits were not exceeded. However, properties such as saturation voltage drop and on-state resistance posed critical implications toward the results of the simulation. Relevant properties were assigned the following values:

Diode Saturation Voltage Drop: 1.0 V

Diode On-state Resistance: 0.001  $\Omega$

IGBT Saturation Voltage Drop: 1.0 V

IGBT On-state Resistance: 0.001  $\Omega$

It was also assumed that the energy lost in turn-on was equal to the energy lost in turn off, and was related to collector current through the following expression:

$$E_{Switch} = (3.288 * 10^{-4}) |I_{Collector}| + .041 \text{ Joules} \quad (3.1)$$

The Psim model used to represent the IGBT will be discussed later in this chapter.

### 3.3 Top Level Dynamic Wind Cascaded H-Bridge Model

The model of the single leg of the cascaded H-bridge inverter, along with its controls, was constructed in Psim, using blocks to represent various components. This model featured extra control functionality necessary to operate a wind farm under dynamic wind conditions. The diagram in Figure 3.1 shows ideal DC sources representing the power output of each SDCS, battery DC sources representing the analog voltage (and thus power stored) output signal of wind turbines, 5 blocks representing 5 H-bridges, and one block representing the overall controller of the wind farm. The overall controller sends two gating signals to each H-bridge, one controlling the positive half cycle and one controlling the negative half cycle. The top-level diagram is shown below in Figure 3.1.

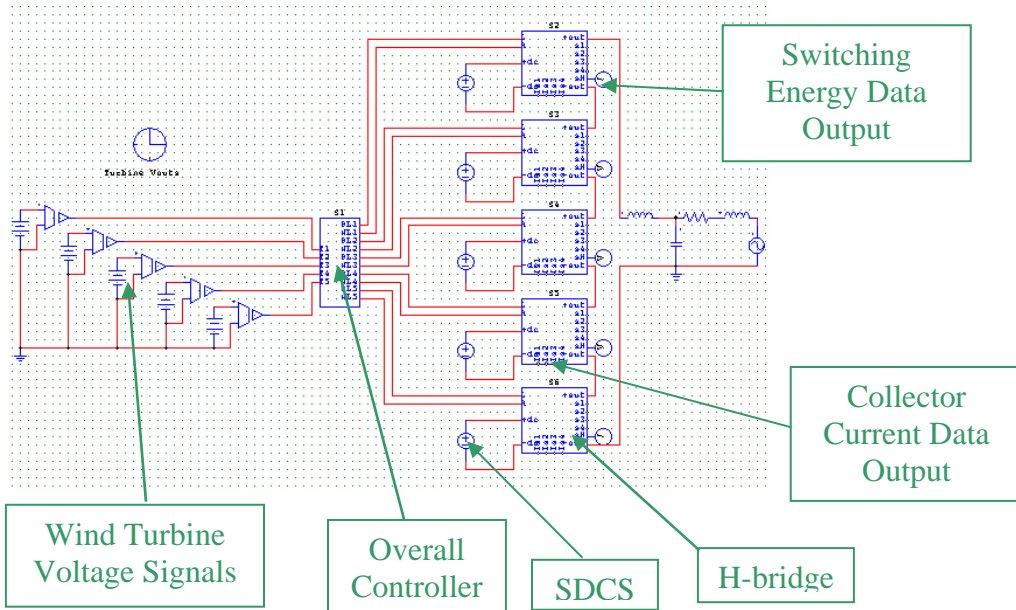


**Figure 3.1** Top-level model of the inverter, without the output line filters

### **3.4 The Controller**

The controller block, shown in Figure 3.2, includes sine-triangle generators, with a 5 kHz switching frequency, a clock signal generator, and a rank assignment block. The sine-triangle generators create unranked gating signals that are fed into the rank assignment block (the “rank” issue will be discussed later). The clock is generated from the reference voltage. It is used to synchronize the ranking control with the reference voltage, and thus insure that the rank of an SDCS is not changed in the middle of a line cycle.

### **3.5 The Rank Assignment Block**

Due to the unpredictable nature of wind, the issue of rank is crucial in the control of this inverter. Because the turbines throughout a wind farm are subjected to different wind conditions, power output can vary amongst them. In a cascaded H-bridge inverter, the SDCS that is assigned to the top and bottom levels of the approximated sine wave does not provide as much power as the SDCS assigned to the middle levels. Therefore, an objective of this control is to rank the turbines based on power production, and then assign them to a level accordingly. This control accomplishes that through comparators and digital logic, which are contained in the rank assignment block, as shown in Figure 3.3. The unconditioned output voltage signals (representing power production) are fed into a block that consists of an array of comparators, called the “comparator array,” which compare each phase to one another. The outputs of all the comparators are then fed to multiplexer drivers. There is one multiplexer driver for each wind turbine SDCS, driving two multiplexers, with each switch either the positive or negative half cycle

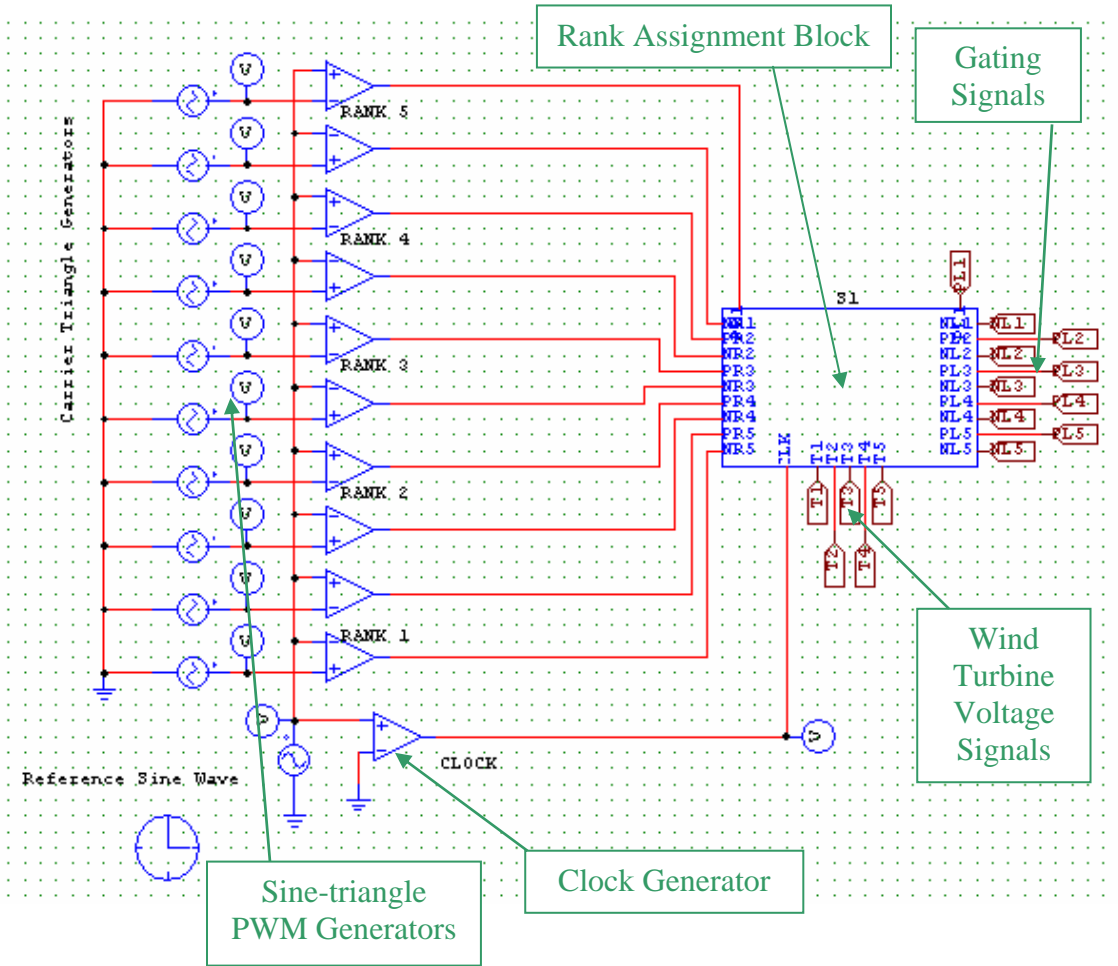


**Figure 3.2** The controller block

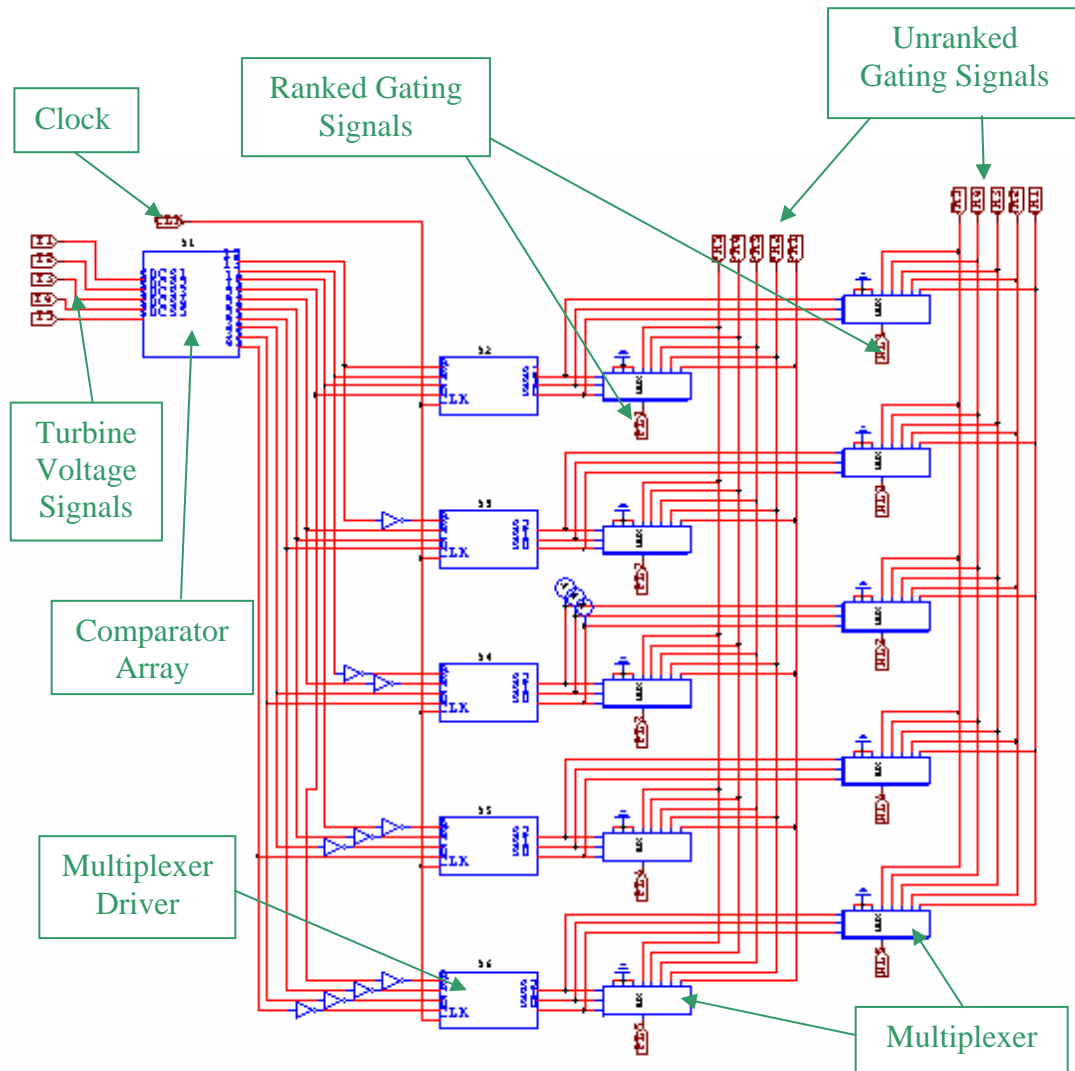


**Figure 3.3** The rank assignment block

gating signals to the corresponding H-bridge. Since a multiplexer driver corresponds to a given turbine with a given output, it only needs to know how its turbine's output compares to the others. Then each multiplexer's output represents either the positive or negative half-cycle gating for a specific H-bridge in the overall inverter. The overall purpose of this block is to decide which gating signals go to which H-bridge corresponding to a fixed turbine.

### **3.6 The Comparator Array**

The purpose of the comparator array is to rank each turbine in terms of power production. It accomplishes this through a series of comparators. This array takes in the analog voltage readings of each turbine's DC link capacitor, and then compares them to each other. For a given turbine, this block will determine if its power production is higher or lower than that of all of the other turbines. It then outputs binary signals that represent the results of this comparison. The topology of the comparator array is shown in Figure 3.4.

### **3.7 The Multiplexer Driver**

The purpose of the multiplexer driver is to convert the four bits of ranking information from the comparator array into three bits that can instruct the multiplexers as to how to switch. It accomplishes this conversion through combinational digital logic. After the conversion occurs, the output bits are sent to D flip-flops, which are synchronized relative to the clock that was generated from the original line voltage reference signal. The purpose of these flip-flops is to insure that a change in rank will not

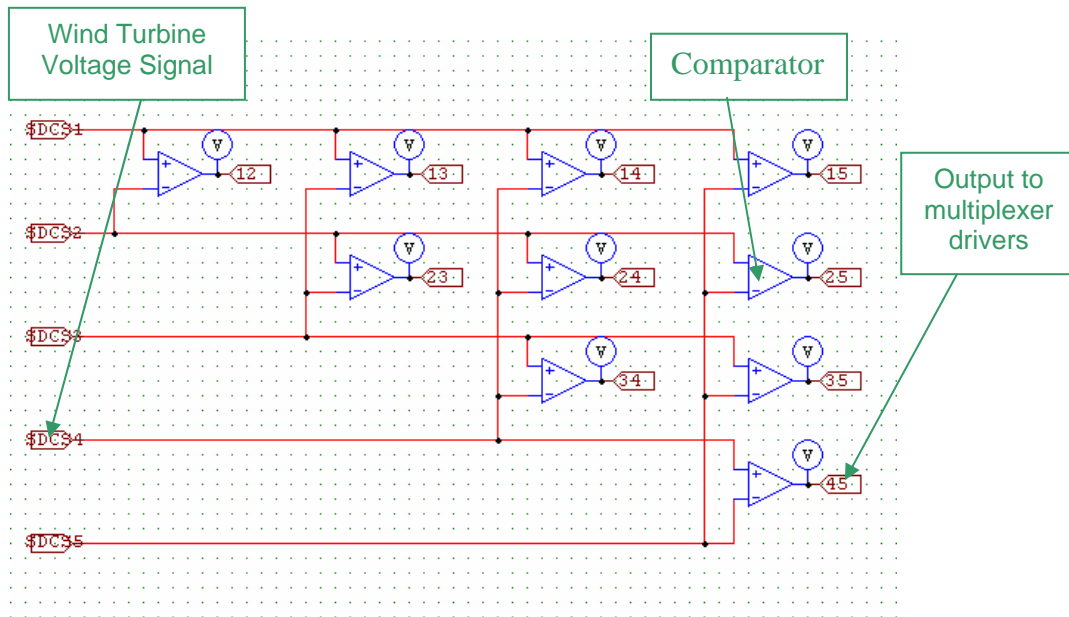


**Figure 3.4** Topology of the comparator array

occur during the middle of a line cycle. These flip-flops presented a minor imperfection in the model. Because they did not actually see an active clock edge at the beginning of the simulation (the clock began at a high value, as opposed to transitioning from low to high), the flip-flops did not take in the value they needed to until the beginning of the second line-cycle. Therefore, the output of this model was not valid for the first line-cycle (this was one reason why a separate model was created to study issues related to efficiency and component sizing).

It can be seen in Figure 3.5 that there are not-gates in the inputs to some of the multiplexer drivers. This is to cut down on the number of comparators needed in the comparator array. Conceptually, the multiplexer driver takes in the information of “how does this turbine compare to the others.” The purpose of the not-gates is to convert “how do others compare to this turbine” to “how does this turbine compare to others.” The reason for putting these not gates into the rank assignment block, as opposed to the multiplexer driver, was so that each of the five multiplexer driver blocks would be identical on the inside. The topology of the multiplexer driver block is shown in Figure 3.5.

### **3.8 H-bridge and IGBT**

In the top-level diagram of the inverter, each H-bridge module is contained in a single block. Although the H-bridge is a well-known topology (it is still shown in Figure 3.6), some details relating to the IGBTs should be discussed at this point. In Psim, the only

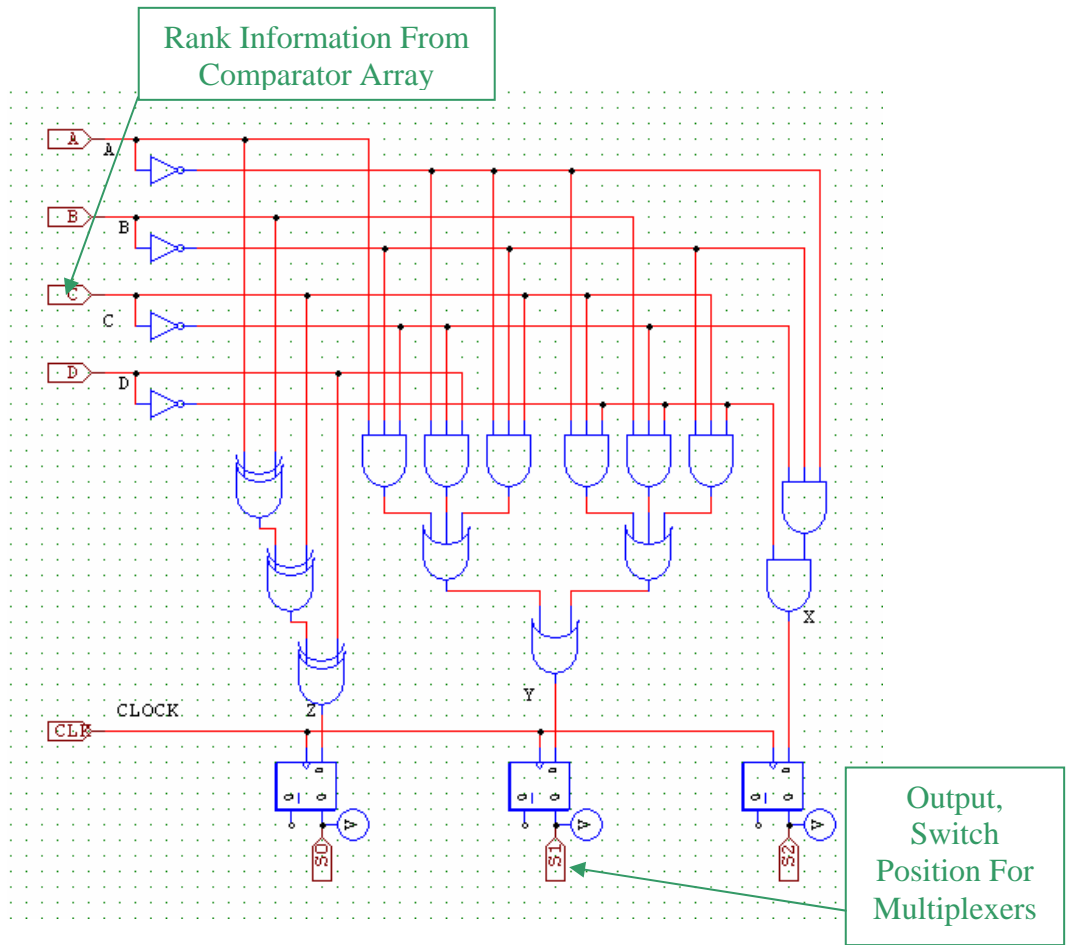


**Figure 3.5** Multiplexer driver block

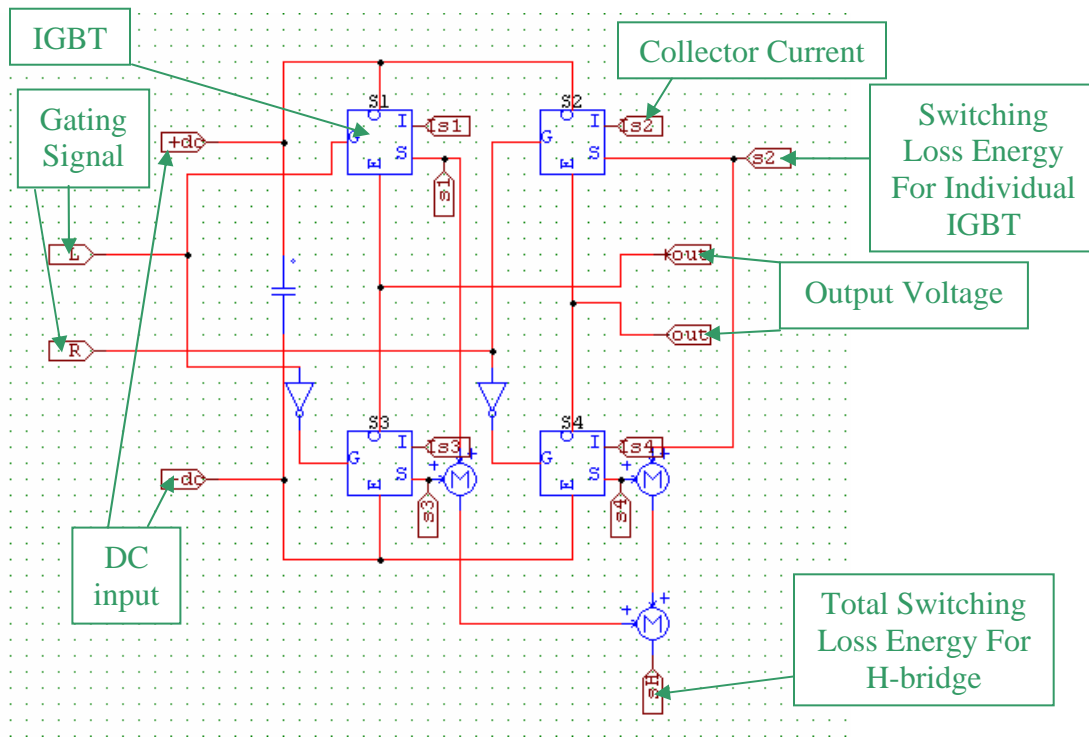


**Figure 3.6** The topology of the H-bridge block

parameters that can be assigned to an IGBT are the on-state voltage drop and diode voltage drop. Therefore, blocks representing each IGBT are shown in Figure 3.6. In order to take into account conduction losses, a resistor was added in series with the IGBTs, as shown in Figure 3.7.

The model of the IGBT, shown in Figure 3.7, must perform four tasks during the simulation. The first and second tasks, to turn on and off when commanded, and introduce an on-state voltage drop across the bypass diode and IGBT, are accomplished automatically through the Psim Software. The third task, which is to model conduction losses of both the IGBT and bypass diode, is accomplished by inserting a resistor in series with the IGBT. The fourth task, to compute the energy lost each time the IGBT changes between the on and off state, involves a much more complex model.

The functions of the model can be broken into two subgroups: determining energy loss as a function of current, and determining when the IGBT transitions between the on and off state. Determining energy loss as a function of current was done simply through a linear expression that was derived through examining data sheets of typical IGBTs. This equation represented an average of typical turn-on and turn-off loss equations (derived by examining IGBT datasheets), so that it could be accurately assumed that turn-on loss is equal to turn-off loss. This equation needed to be based upon the absolute value of current, to avoid the possibility of negative current resulting in negative energy values being derived. The following equation, which was introduced earlier in the chapter, was derived (by examining IGBT datasheets) for switching energy as a function of current:

$$E_{Switch} = (3.288 * 10^{-4}) |I_{Collector}| + .041 \text{ Joules} \quad (3.1)$$

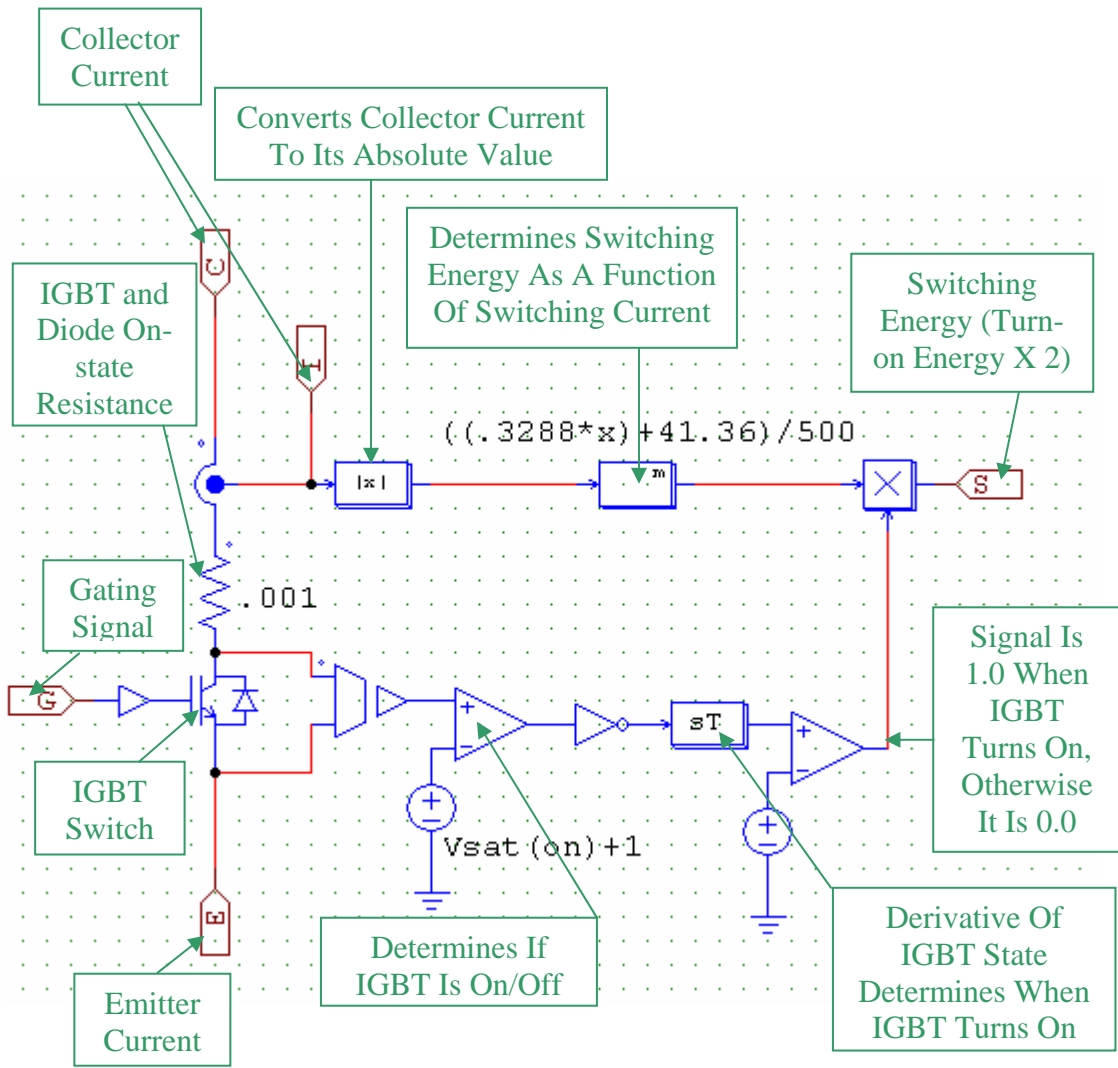


**Figure 3.7** Model of the IGBT, including switching losses

The other portion of the model needed to determine when a switching event took place and output a value of one at that instant in time, while outputting a value of zero at all other times. Then that signal could be multiplied by the output of the block that continuously outputs switching energy as a function of current, thus yielding a final amount of switching energy only when a switching event occurred. The first step in this process was to determine when the IGBT was on and off. This was done by measuring the voltage across the IGBT, and then comparing it to a number that was slightly above the saturation voltage value of the IGBT (recall that this saturation voltage was input by the user), thus yielding a binary 1 when the IGBT was off, and binary 0 when the IGBT was on. The signal had to be run through a not-gate, so that future blocks would detect turn-on, as opposed to turn-off. This needed to be done because Psim would reduce the current through the transistor to its on-state leakage value one time-step before the model detected the turn-off event, thus giving an artificially low value for turn-off energy. This problem was avoided by only detecting the turn-on events, and multiplying the energy as a function of current expression by two, in order to yield the sum of both turn-on and turn-off events simultaneously.

The IGBT state signal was then run through a differentiating block, which would output a positive spike when the signal turned on, and a negative spike when the signal turned off. In order to insure that the spike was always equal to a magnitude of 1, so that it could be multiplied by the energy as a function of current signal, the spike was compared to a number slightly above zero. With its value equal to 1 at the appropriate time, the signal was then multiplied by the energy, thus outputting the sum of the turn-on and turn-off energy whenever the IGBT turned on. In order to access this information,

the text file that Psim created whenever it ran a simulation would be opened in a spreadsheet program, at which point all of the discrete switching energies could be added to get the total switching energy lost over the simulation, which could then be divided by the simulation time, to yield a single number for the average power lost to switching.

It should be noted that the IGBT model shown in this thesis could be modified to represent any power-electronic switch. All that is required is to change the IGBT in the model to the desired switch, change the on-state resistance to the appropriate value, and then change the current to energy equation to fit the desired device.

### **3.9 Utility Interface**

All inverter models created in this thesis contained a utility interface. This consisted of a voltage source, inductor, and resistor that represented the impedance and voltage of the line. The values of this utility impedance could be manipulated to represent varying line lengths. The phase angle of the voltage source was also manipulated to control the flow of real power from the inverter. The interface also consisted of a series inductor, shunt capacitor filter located between the utility impedance and inverter, as shown in Figure 3.8. A similar, three phase Y-connected model was constructed for the full-bridge inverter.

### **3.10 Cascaded H-Bridge Inverter Model for Efficiency and Component Size**

Although the model created for dynamic wind conditions was capable of yielding the information needed for a study of efficiency and component sizing issues, a separate model was created for these simulations. This was done simply to reduce the time required to run the simulation, and in order to ease the interpretation of results by not

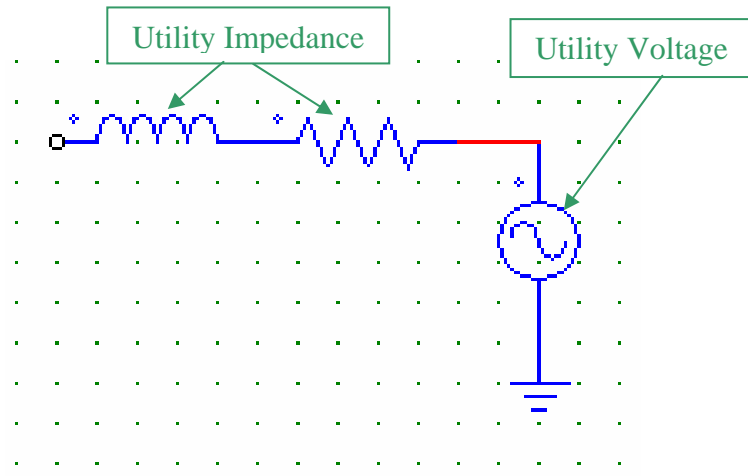


**Figure 3.8** The model of the utility interface

having to consider the issues related to the flip-flops in the multiplexer-driver not being set during the first line-cycle.

This model featured the cascaded H-bridges being driven directly by sine-triangle generators, without the rank assignment functionality between them. This was an acceptable shortcut since the rank assignment functionality was not necessary for a study of efficiency and component sizing issues. The topology used is shown in Figure 3.9.

### **3.11 Full-Bridge Inverter Model**

A model of a wind turbine with a single full-bridge inverter was also created. This was done in order to compare the efficiency of the cascaded H-bridge inverter, which represented a new method of converting wind farm output, to a way that represented the present method of converting power. Since present wind farms use only one inverter for every turbine, it was not necessary to compare an equal number of full-bridge inverter paired to turbines to the number of turbines used in the cascaded H-bridge inverter. Like the H-bridge efficiency model, the full-bridge model used the same IGBT models that calculated all major losses, including the switching losses. A top-level topology of the full-bridge inverter model, including the output filter, utility interface, and same IGBT models that were used in the cascaded H-bridge model, is shown in Figure 3.10.

Three models have been created in order to evaluate the efficiency and component sizing issues of the cascaded H-bridge inverter, to evaluate its performance under dynamic wind conditions, and to establish a baseline for comparison with the full-bridge inverter, which is commonly used in wind farms today. With these models created,

Rank assignment functionality is eliminated, so sine-triangle generators drive the H-bridge modules directly

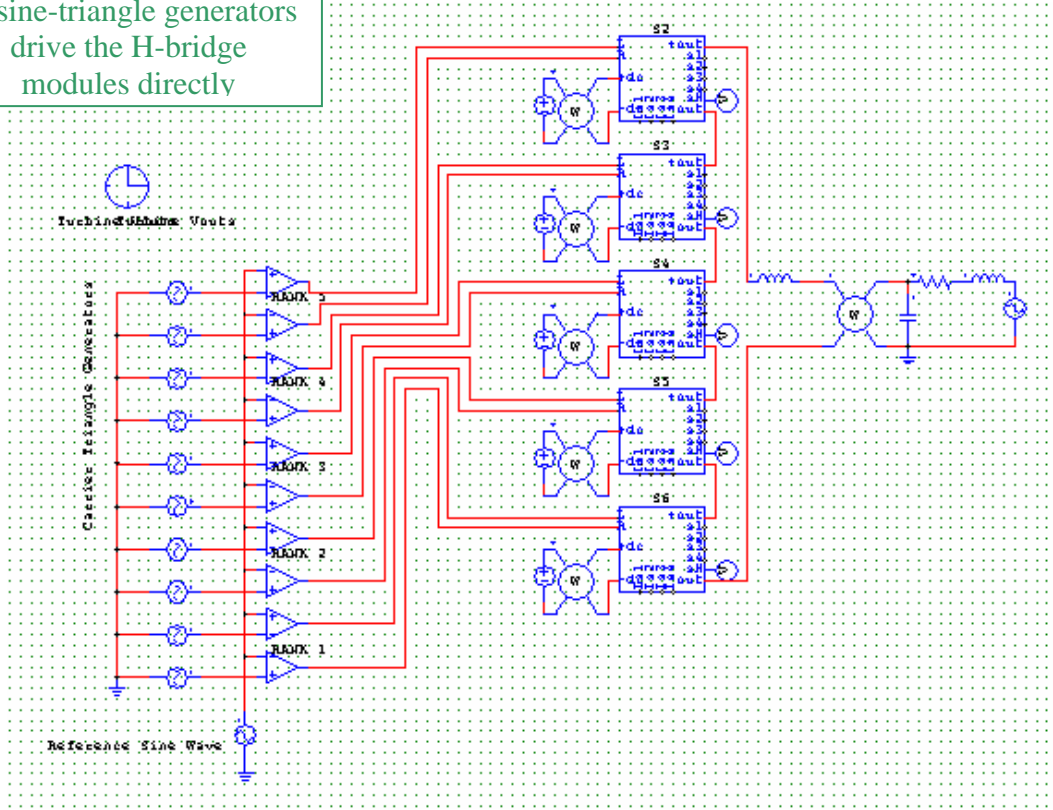


**Figure 3.9** Cascaded H-bridge model with simplified control used for efficiency and component sizing studies

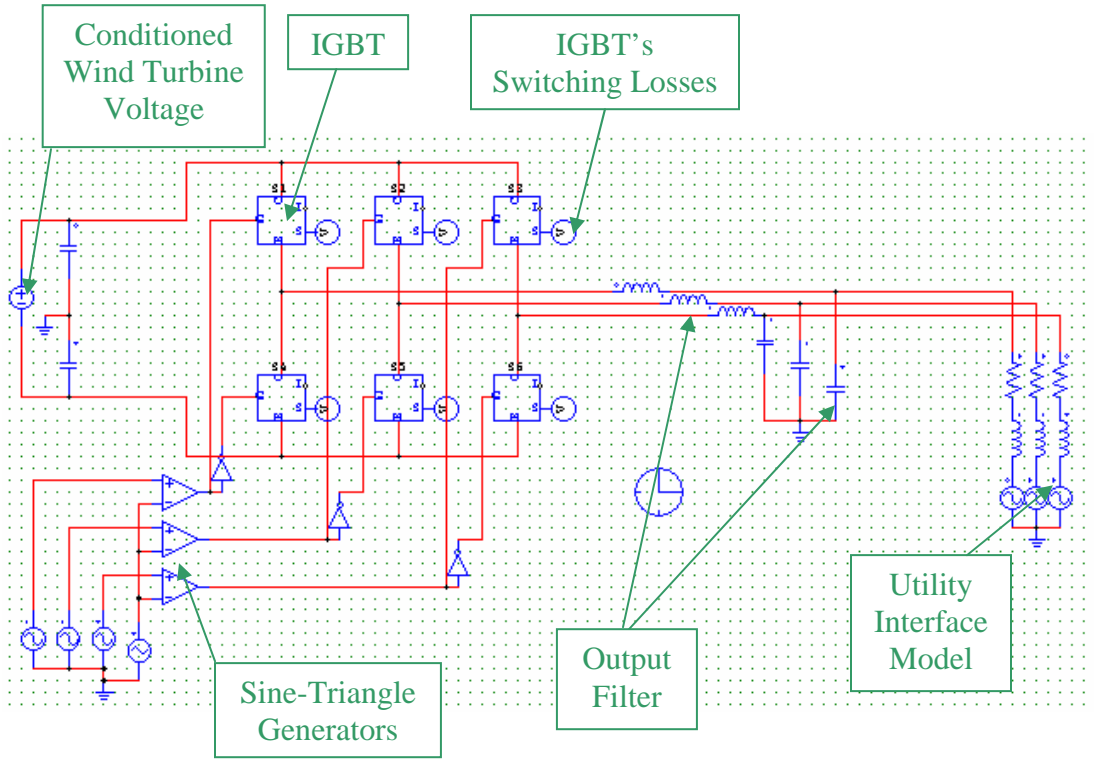


**Figure 3.10** The full-bridge model's topology

simulations were run to determine how well suited the cascaded H-bridge multilevel inverter would be for wind farm application. The results of these simulations will be discussed in the next chapter.

## **4 RESULTS**

With the cascaded H-bridge and full-bridge inverter models completed, a number of simulations were run. These simulations were primarily intended to yield information that would be relevant to an evaluation of the economics of the cascaded H-bridge versus the standard full-bridge. Secondary consideration was given to control under dynamic conditions.

Economics related to the power-electronic switches (IGBTs in this case) remained the ultimate parameter of study. Primary switch considerations evaluated included converter efficiency, which would have an effect on the cooling systems required and lifespan of the power-electronic switch, along with the size of the collector current experienced by the IGBTs, which would have an effect on the ratings of the power-electronic switches required. The simulations run were thus designed to yield information about converter efficiency and collector current experienced by the switches.

### **4.1 Determining Simulation Parameters**

Since efficiency was a key parameter to be examined, it was important that the SDCSs in the cascaded H-bridge inverter have the same voltage as the single DC source in the full-bridge inverter. For a given commanded power output, a DC source with lower voltage would produce more current than one with a higher voltage would. This higher current would cause both conduction and switching losses to increase, since both are proportional to current magnitude. Therefore, DC source voltages need to be kept the

same so that higher current levels would not skew results. A DC source voltage of 4,000 V was arbitrarily chosen (within the bounds of reasonable values).

Another critical parameter to be chosen was the commanded power output. Four values were chosen: 750 kW, 1250 kW, 1750 kW, and 2250 kW for the full-bridge simulation. These values were chosen because they were evenly distributed within the range of power outputs of the best-selling utility scale wind turbines on today's market (1.8 MW models from Vestas and 1.5 MW models from General Electric dominate current sales in the United States). The power output was manipulated by altering the phase angle of the converter output voltage relative to the utility voltage. The following equation demonstrates how two voltage sources, a sending source and a receiving source, connected through an impedance X, send an amount of real power that can be manipulated by altering voltage phase angle. This equation was used to determine the phase angle required for the desired power flow.

$$P = \frac{V_{send} V_{receive}}{X_{line}} \sin(\delta_{send} - \delta_{receive}) \quad (4.1)$$

A critical consideration in determining parameters was to keep as many of them the same in both the full-bridge and cascaded H-bridge simulations as possible, thus exposing each DC power source to identical (or near identical) conditions. Therefore, the four commanded power values used in the full-bridge simulations needed to be multiplied by five to attain the proper power output values for the cascaded H-bridge simulations (since the total output power of the cascaded H-bridge model contained the output power of five different wind turbines).

The actual power that was produced by the inverters was somewhat less than what was commanded, due primarily to the fact that the equation used to estimate power-flow did not take line impedance into account (it only considered the impedance due to the filter inductor), while the utility interface models did take line impedance into account. Efforts were not made to compensate for these in terms of the utility phase angle because as long as the output power was recorded within range of typical utility scale wind turbines, and taken into account in calculations, its actual value was somewhat arbitrary.

#### 4.2 Full-Bridge Efficiency Simulations, A Baseline for Comparison

The first simulations to be performed involved an evaluation of the full-bridge inverter, which is the type of inverter commonly used in wind farms today. Four different simulations were run, in which overall efficiency, conduction losses, and switching losses were computed. The results of these four simulations are shown in Tables 4.1 and 4.2.

**Table 4.1** Results of simulations run with full-bridge inverter at various power levels

<u>Pcommanded (kW)</u>	<u>Psent (W)</u>	<u>Ploss (W)</u>	<u>Efficiency (%)</u>	<u>Pswitch (W)</u>	<u>Pconduction (W)</u>
750	714146	39413	94.481	5796	33617
1250	1194091	62864	94.735	8346	54518
1750	1666512	79972	95.201	10767	69205
2250	2056562	98776	95.388	13438	85338

**Table 4.2** Breakdown of total power loss into conduction and switching losses

<u>Pcommanded (kW)</u>	<u>Ploss (W)</u>	<u>% lost in Switching</u>	<u>% lost in Conduction</u>
750	39,413	14.7	85.3
1,250	62,864	13.3	86.7
1,750	79,972	13.5	86.5
2,250	98,776	13.6	86.4

It can be seen that efficiency increased slightly with output power, ranging from a low of 94.5% at 750 kW commanded to a high of 95.4% at 2250 kW commanded. These values are typical of full-bridge inverters. It can be also seen that, while there is no logical trend in how the breakdown of power loss (into switching and conduction losses) changes with commanded power, conduction losses consistently account for 86% of all power lost, while switching losses account for approximately 14% of all power lost.

### **4.3 Cascaded H-Bridge Inverter Efficiency Calculations**

Having established a baseline for comparison by simulating the full-bridge inverter, the cascaded H-bridge inverter was then simulated to calculate its efficiency. This was done using a simple H-bridge model, which did not have the extra control features that would be necessary to operate under dynamic wind condition (specifically, the ability to assign SDCSs varying ranks). This control feature was left out because it increased computational complexity without adding information or capabilities that would be necessary for a study of efficiency.

With the parameters that would most accurately parallel those from the full-bridge simulations determined, four simulations were run of the same cascaded H-bridge inverter model, each with a different output power level commanded (by altering the phase angle of the utility voltage). The results of the efficiency simulations are presented in Tables 4.3 and 4.4 and Figure 4.1. The losses calculated in these H-bridge simulations are then compared to those from the full-bridge simulations in Table 4.5.

**Table 4.3** Results of the efficiency calculations, including output power without switching losses, input power from each H-bridge, total input power, switching energy from each H-bridge, total switching energy, power lost in switching, total output power, power lost to conduction, and overall converter efficiency

<b>Pcommanded</b>	<b>3750K</b>	<b>6250K</b>	<b>8750K</b>	<b>11250K</b>
<b>Pout (W)</b>	2,902,935	5,105,697	7,398,256	9,661,709
<b>Pin H1 (W)</b>	770,231	1,334,005	1,937,852	2,528,032
<b>Pin H2 (W)</b>	740,925	1,284,051	1,862,166	2,429,141
<b>Pin H3 (W)</b>	672,883	1,167,627	1,692,676	2,208,910
<b>Pin H4 (W)</b>	553,680	963,227	1,393,722	1,818,696
<b>Pin H5 (W)</b>	318,377	555,781	800,534	1,043,858
<b>Pin total (W)</b>	3,056,097	5,304,694	7,686,953	10,028,639
<b>Energy H1 (J)</b>	62.24	60.93	66.59	68.2
<b>Energy H2 (J)</b>	63.67	64.58	75.97	81.44
<b>Energy H3 (J)</b>	78.91	89.56	110.27	128.07
<b>Energy H4 (J)</b>	99.11	121.97	158.65	194.52
<b>Energy H5 (J)</b>	236.5	334.87	452.44	568.69
<b>Energy Total (J)</b>	540.43	671.91	863.92	1040.93
<b>Pswitch (W)</b>	2,705.13	3,359.54	4,319.58	5,204.64
<b>Pout total (W)</b>	2,900,233	5,102,338	7,393,937	9,656,505
<b>Pconduction (W)</b>	153,162	198,997	288,696	366,930
<b>Efficiency</b>	0.949	0.962	0.962	0.963

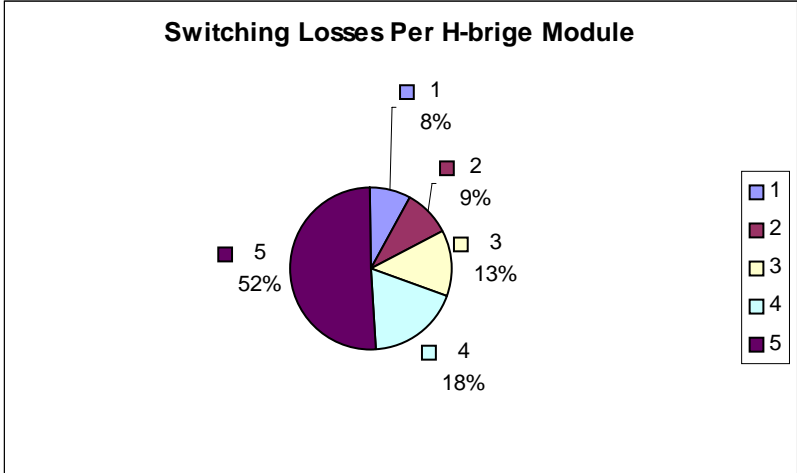


**Figure 4.1** Percentage of total switching losses per level. 5 represents the H-bridge at the top and bottom of the waveform, while 1 represents the H-bridge at the middle of the waveform

**Table 4.4** Breakdown of total power loss into switching and conduction losses

<b><u>Pcommanded</u></b>	<b><u>3750K</u></b>	<b><u>6250K</u></b>	<b><u>8750K</u></b>	<b><u>11250K</u></b>
<b>Pswitch (W)</b>	2,705	3,359	4,319	5,204
<b>Pconduction (W)</b>	153,162	198,997	288,697	366,930
<b>Ptotal loss (W)</b>	155,867	202,356	293,016	372,134
<b>Switch % total</b>	1.7	1.7	1.5	1.4
<b>Conduction % total</b>	98.3	98.3	98.5	98.6

**Table 4.5** Comparison of losses in full-bridge and cascaded H-bridge inverters

<i>Inverter Type</i>	<i>H-bridge</i>	<i>Full</i>	<i>H-bridge</i>	<i>Full</i>
Pcommanded (kW)	3750	750	6250	1250
Efficiency	0.949	0.945	0.962	0.947
Switching % Total	<b>0.017</b>	<b>0.147</b>	<b>0.017</b>	<b>0.133</b>
Conduction % Total	<b>0.983</b>	<b>0.853</b>	<b>0.983</b>	<b>0.867</b>
<i>Inverter Type</i>	<i>H-bridge</i>	<i>Full</i>	<i>H-bridge</i>	<i>Full</i>
Pcommanded (kW)	8750	1750	11250	2250
Efficiency	0.962	0.952	0.963	0.954
Switching % Total	<b>0.015</b>	<b>0.135</b>	<b>0.014</b>	<b>0.136</b>
Conduction % Total	<b>0.985</b>	<b>0.865</b>	<b>0.986</b>	<b>0.864</b>

It can be seen from the results that the most dramatic results are in the reduction of switching losses in the cascaded H-bridge inverter. While switching losses consistently make up around 14% of all losses in the full-bridge inverter, they make up only about 1.5% of total losses in the cascaded H-bridge inverter. Conduction losses per wind turbine are also slightly reduced in the cascaded H-bridge inverter over those of the full-bridge inverter (as can be seen when comparing conduction losses in Tables 4.1 and 4.3). In terms of overall efficiency, the cascaded H-bridge inverter tends to be about 1% point higher than the full-bridge inverter. The main advantage of the cascaded H-bridge, in the realm of efficiency, is a reduction in switching losses. These make up a fairly small portion of total losses, so their reduction does not have as strong of an impact on

overall efficiency as a reduction in conduction losses would. It is also shown that the further away an H-bridge module is placed in the output waveform from the middle (in terms of rank), the greater its switching losses will be. This makes sense because as an H-bridge module is placed closer to the outside, it will experience more switching events per line-cycle.

#### **4.4 Full-Bridge Simulations For Component Sizing**

In order to understand the demands for component sizing, a study of instantaneous current needed to be executed. While voltage-sizing requirements of a switch are easily pre-determined based upon the design parameters of a converter, the current requirements can best be determined through simulation. Therefore, the collector currents experienced by each switch were monitored during the simulations of the full-bridge inverter.

For ease of comparison, the output currents at the lowest and highest commanded output powers will be examined. It can be seen from Figures 4.2 and 4.3 that, when 750 kW is commanded, the current peaks around 450 A, while rarely exceeding 400 A. And when 2,250 kW is commanded, the current peaks around 1,300 A.

#### **4.5 Cascaded H-bridge Simulations For Component Sizing**

Collector currents on the IGBTs in the cascaded H-bridge inverter were examined next. Currents were examined for each switch in the H-bridge module positioned at the outside of the output waveform and for each switch in the H-bridge module positioned in

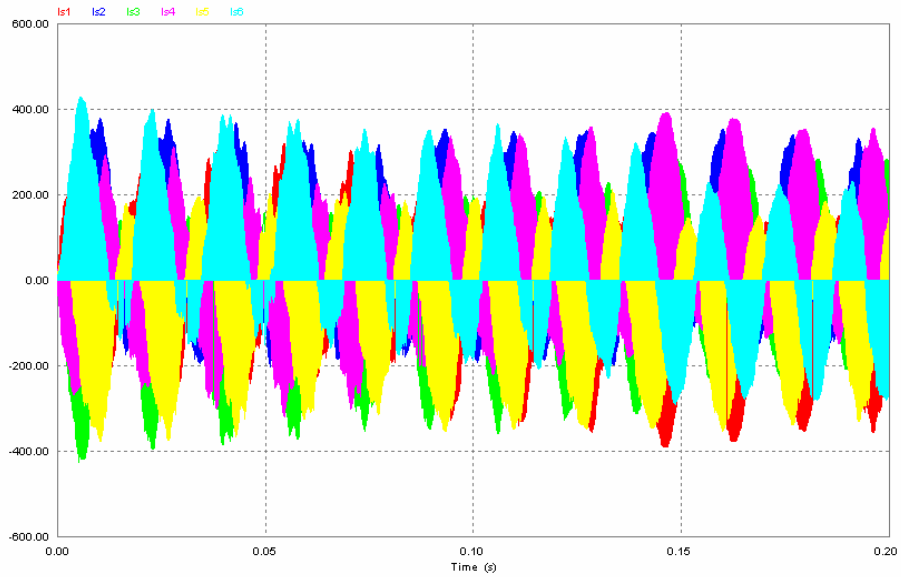


**Figure 4.2** Instantaneous collector currents (in Amps) experienced by all six switches during the operation of the full-bridge inverter at 750 kW commanded

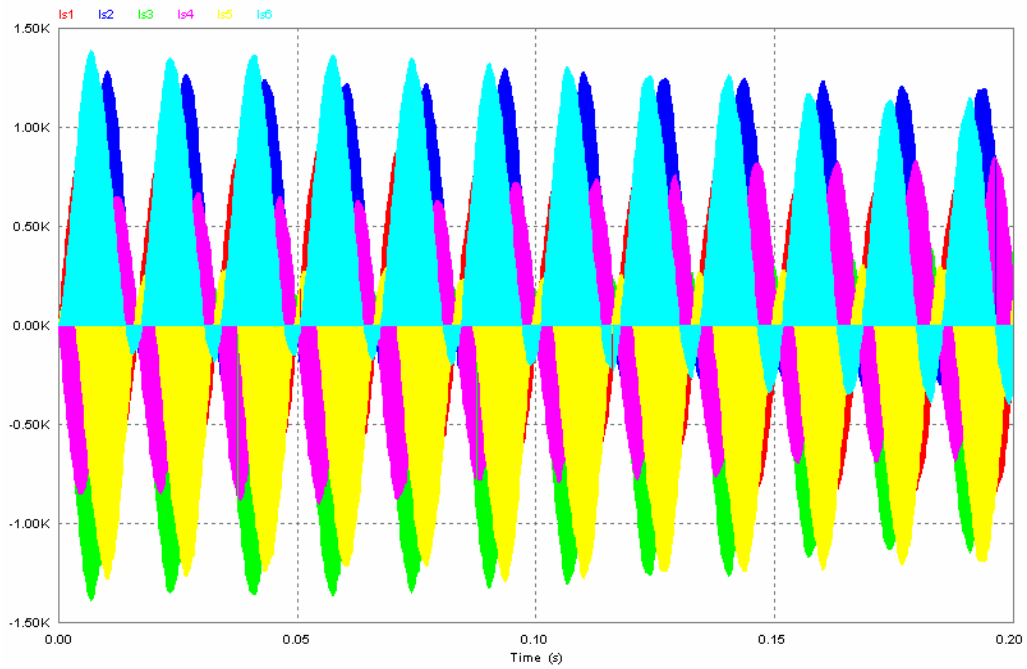


**Figure 4.3** Instantaneous collector currents (in Amps) experienced by all six switches during the operation of the full-bridge inverter at 2,250 kW commanded

the middle of the output waveform. Results are shown in Figures 4.4-4.7 for these currents at the highest and lowest commanded output powers.

Figures 4.4, 4.5, 4.6, and 4.7 demonstrate that the peak magnitude of current is close to the same in all levels of the cascaded H-bridge inverter (although not shown, all levels between those two that were shown had similar current waveforms). When each SDCS is providing 750 kW, the current reaches a peak value of around 1,000 A, while when each SDCS is providing 2,250 kW, the current reaches a peak of around 1,800 A.

#### **4.6 Cascaded H-bridge Simulations, Control Under Dynamic Wind**

Having performed simulations to gain an understanding of converter efficiency and switching requirements, simulations had to be performed that would test the converter's performance under dynamic wind conditions. Specifically, these simulations needed to test the ability of the controller to assign an SDCS (wind turbine) to a different rank in the output waveform based upon its power production relative to other SDCSs.

The first simulation to be performed tested whether the controller would assign the wind turbines to the proper rank in the output waveform under static wind (and thus power production) conditions. SDCS 1 was assigned the highest power production (rank #1, it produced the most power out of any of the SDCSs), SDCS 2 was assigned the second highest production (rank #2), SDCS 3 was assigned the lowest production (rank #5), SDCS 4 was assigned the third highest production (rank #3), and SDCS 5 was assigned the second lower production (rank #4).

The output voltage of each H-bridge, in which H-1 is connected to SDCS 1, H-2 is connected to SDCS-2 and so on, is shown in Figure 4.8. The duty cycle of each H-

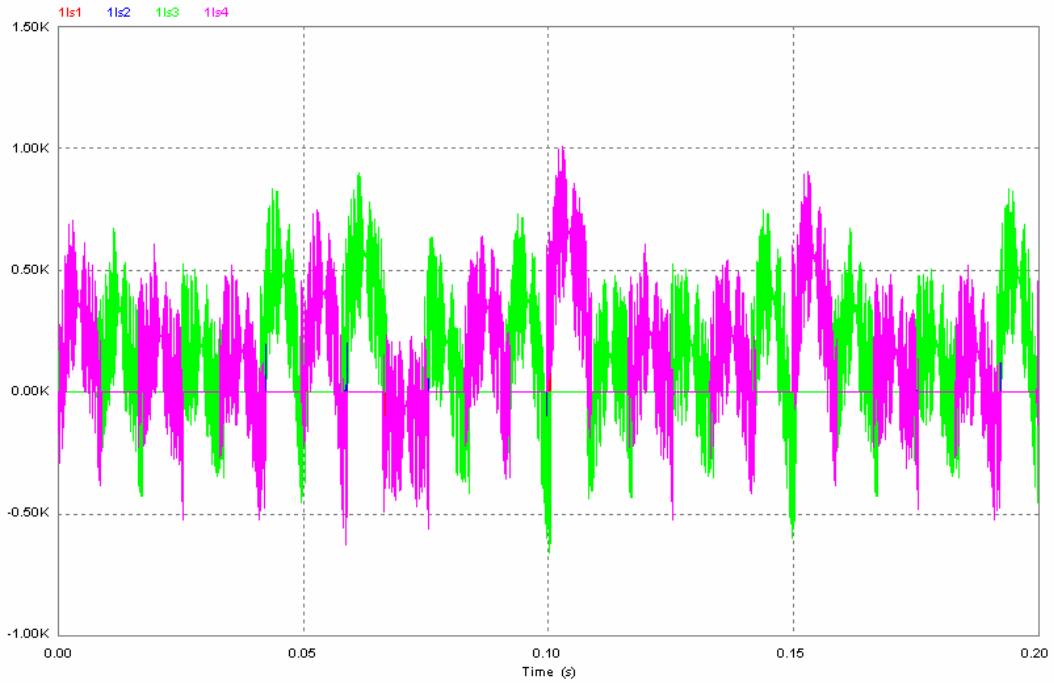


**Figure 4.4** The collector current (in Amps) for all switches in the H-bridge module closest to the middle of the output waveform, when it is commanded to provide 750 kW

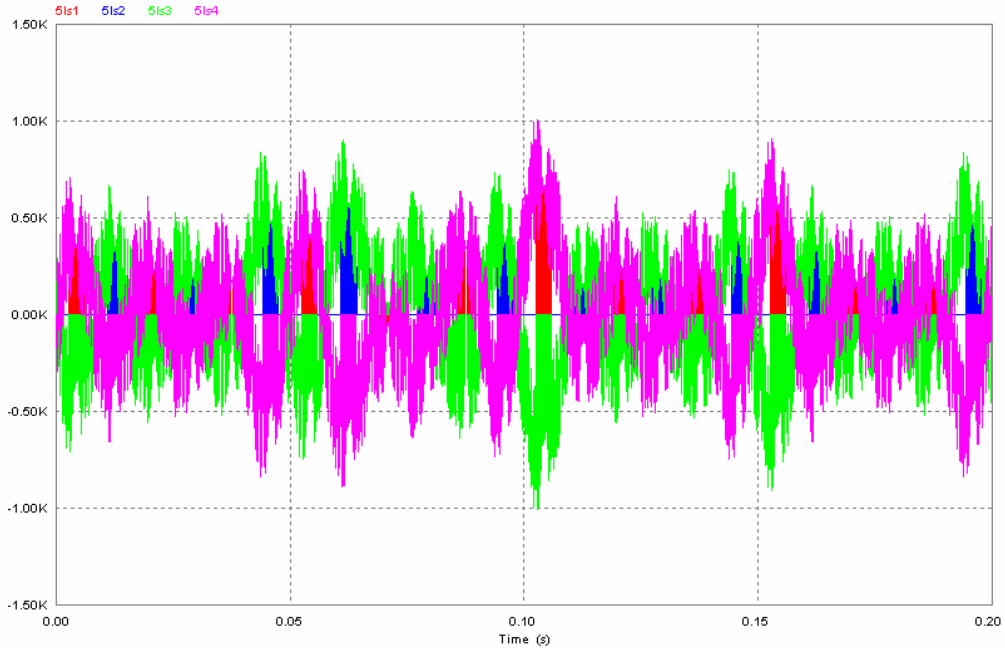


**Figure 4.5** The collector current (in Amps) for all switches in the H-bridge module closest to the outside of the output waveform, when it is commanded to provide 750 kW

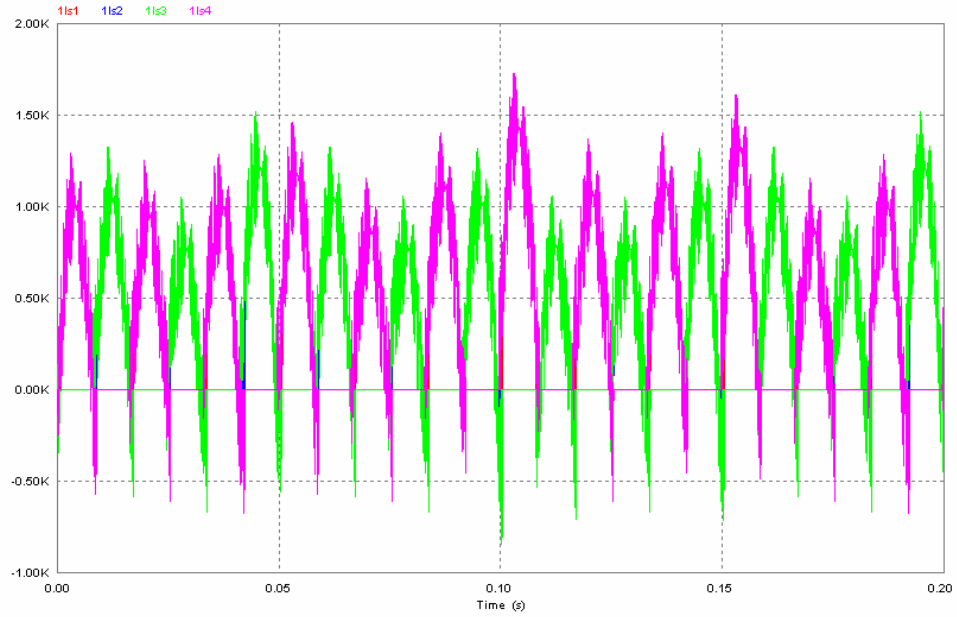


**Figure 4.6** The collector current (in Amps) for all switches in the H-bridge module closest to the middle of the output waveform, when each module is commanded to provide 2,250 kW

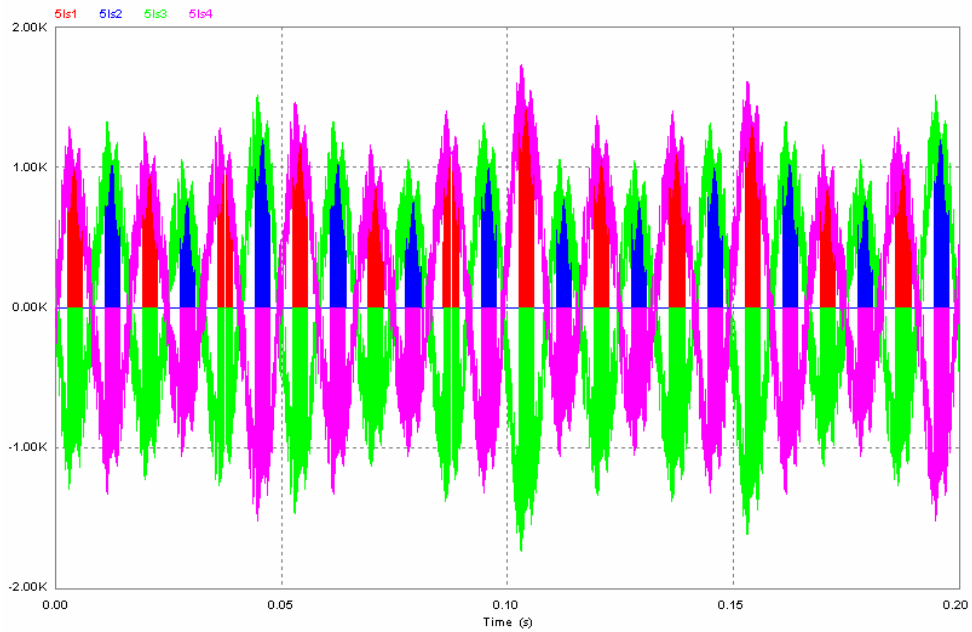


**Figure 4.7** The collector current (in Amps) for all switches in the H-bridge module closest to the outside of the output waveform, when each module is commanded to provide 2,250 kW

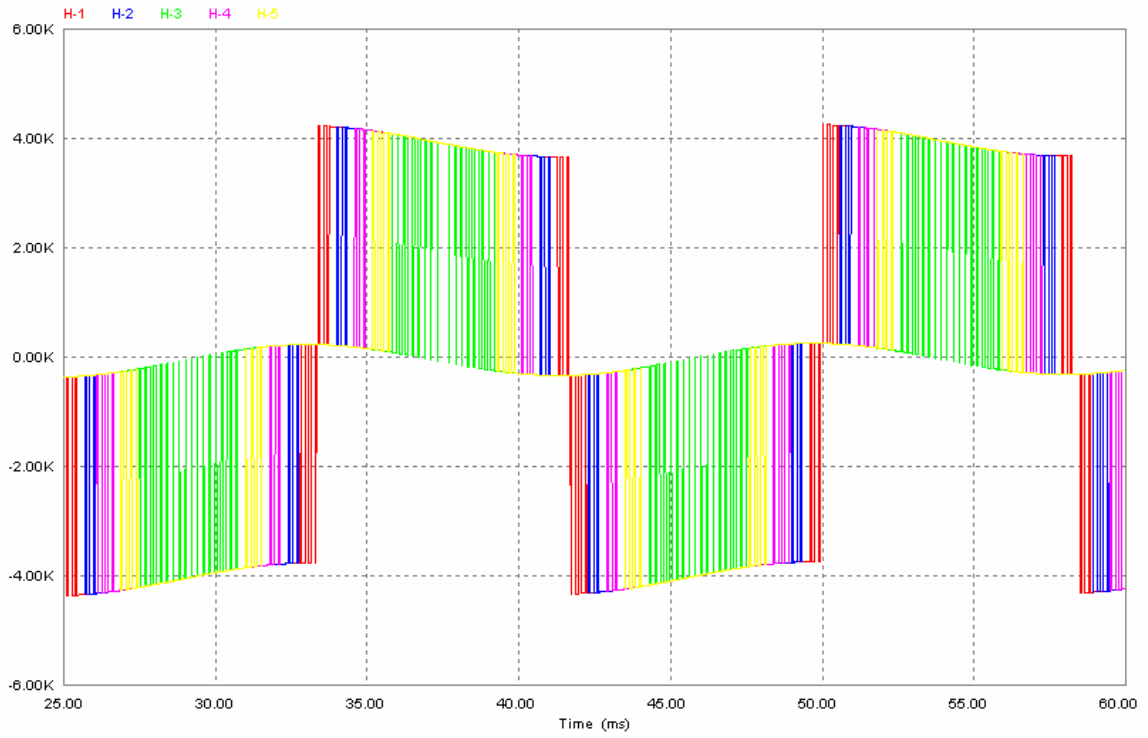


**Figure 4.8** Output voltages of each H-bridge module under static wind conditions

bridge's output represents the time that the H-bridge is on (and thus how much power it contributes to the total output). Thus, the controller will assign the H-bridge connected to the SDCS with the largest power output to the level with the largest duty cycle, and the H-bridge with the smallest power output to the level with the smallest duty cycle, for example. Figure 4.8 shows that H-1 has the largest duty cycle, followed by H-2, H-4, H-5, and H-3, respectively. This order of duty cycle size is the same as the order of the power outputs, so it can be concluded that the ranking control works under static wind conditions.

The controller then needed to be tested under dynamic wind conditions, during which the ranking of output power of some turbines relative to others would change. A simulation was run in which three of the five SDCSs (wind turbines) changed ranks. The ranking of power production is shown in Table 4.6.

**Table 4.6** Power production rankings for each SDCS over the duration of the simulation

<u>Power Production Rank</u>	<u>From 0 to .04s</u>	<u>From .04 to .08s</u>	<u>From .08 to .1s</u>
1	H1	H5	H5
2	H2	H1	H1
3	H3	H2	H4
4	H4	H3	H2
5	H5	H4	H3

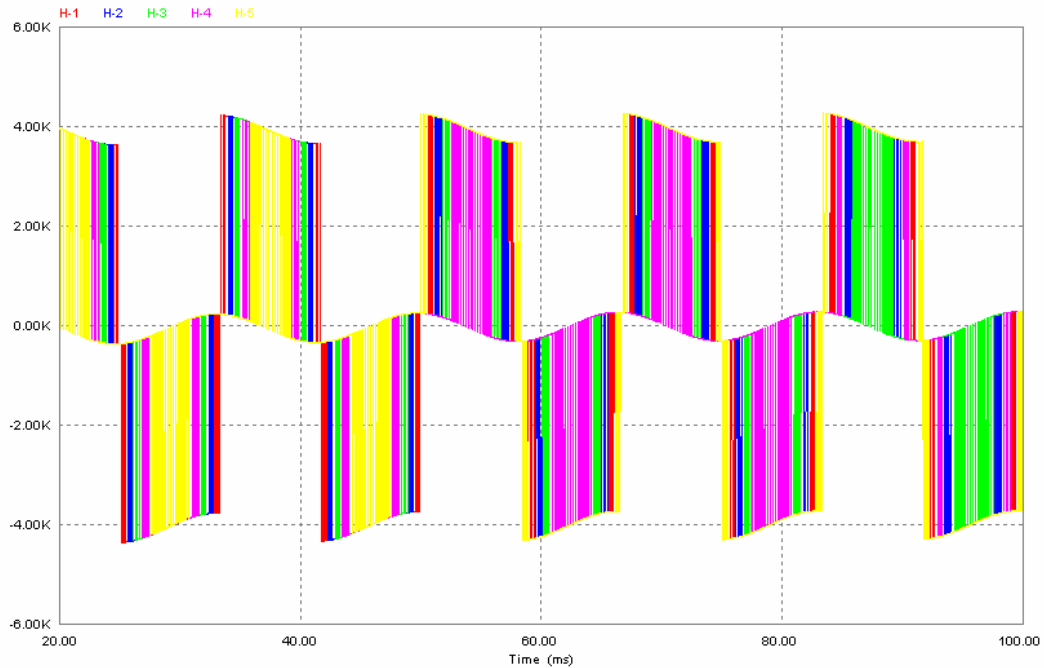


**Figure 4.9** Output voltages of each H-bridge under dynamic wind conditions

The changes in power production rankings during this simulation were designed to test a number of scenarios. This simulation included both increases and decreases in power production rank, and transitions in which one rank changed and others in which multiple ranks changed. It is also important to note that, although the changes in power production rank occurred in the middle of line-cycles, the transitions in terms of rank in output position took place only at the change of line cycles. This demonstrates that the flip-flops in the multiplexer-driver are doing their jobs.

The ranking orders in Figure 4.9 indicate that the control works in a satisfactory manner under dynamic wind/power production conditions. Recalling that the largest duty cycle goes to the SDCS with the largest power production, the second largest duty cycle goes to the SDCS with the second largest power production, and so on, it can be seen that the duty cycles of each H-bridge in Figure 4.9 agree with the rankings described in Table

4.6. The voltage transitions are also free of any significant distortions or overshoots, which indicates that these transitions will not have an impact on stability of the wind farm. It can thus be concluded that the controller works under dynamic wind conditions.

From dynamic characteristics to efficiency and component sizing issues, a wealth of data has been obtained from the simulations that were run. In the next section, that data will be analyzed both to draw conclusions as to the viability of the cascaded H-bridge inverter for wind farms, and to determine what future work needs to take place to further investigate issues brought up in this thesis.

## 5 CONCLUSIONS/FUTURE WORK

### 5.1 Conclusions

The simulations run in Chapter 4 demonstrated that the cascaded H-bridge inverter had superior performance to that of the full-bridge inverter. In the cascaded H-bridge, efficiency was slightly higher, conduction losses were slightly reduced, switching losses were dramatically reduced, the size of the required output filter was reduced, and the need for a transformer to interface to the distribution network was eliminated. In spite of these system-level advantages for the cascaded H-bridge inverter, the amount of current passed through and power dissipated in each switch actually increased in the cascaded H-bridge inverter.

There are two primary potential drawbacks to the cascaded H-bridge inverter. The switches on the cascaded H-bridge will pass more power and current (since the wind turbine's power goes through four switches, as opposed to six on the full-bridge). Addressing this concern was the reason that the component sizing study was done during this simulation. The question is whether reducing the switch count from six to four IGBTs per turbine offsets the fact that the four switches will need to be larger than the six. Another drawback is that, because the output voltage waveform is based upon the sum of the outputs of a series of wind turbines, the cascaded H-bridge topology is less fault-tolerant than the full-bridge based system, in which a series of wind turbines output power to the external grid in parallel to one another. Operating the inverter with a fewer levels than SDCSs that are available, and simply rotating a few SDCSs out during every line cycle can overcome this drawback. Assuming that the DC-link capacitor on the

output of each turbines rectifier would store the energy, each turbine would output more energy while it was in the rotation and then store the power it produced while it sat out. The geographical layout and amount of turbines in a wind farm will need to be taken into account, and if this cascaded H-bridge system is to be implemented in a wind farm, it is possible that some of the turbines may still need to be interfaced through the full-bridge inverter, to keep the number of turbines on each phase equal.

As was shown in the dynamic wind condition/power production simulations, the ability of the control to change the rank, in the output waveform, of a given SDCS is quite satisfactory. Whether one or multiple turbines changed rank, the transition took place smoothly and occurred only at the change of a line cycle. Although this controller used digital logic, it can be concluded that the satisfactory results shown in this thesis would hold if the same control was implemented using sequential software.

Although improvements in efficiency and loss reduction were present, they were not great enough to justify use of the cascaded H-bridge system. On average, the efficiency of the cascaded H-bridge inverter was 1% greater than the full-bridge inverter at each power level. The most dramatic advantage to the cascaded H-bridge was in how it reduced switching losses. However, the amount of power lost to switching in the base case (full-bridge) was small when compared with the power lost in conduction to begin with, so significant improvements in switching losses would not translate into dramatic overall improvements. Considering that each wind turbine was commanded to provide between 750 kW and 2,250 kW, this 1% improvement can represent between 7.5 kW and 22.5 kW less losses per H-bridge, which translates to between 1.875 kW and 5.626 kW less losses per switch.

The ultimate reason for studying efficiency is to understand the thermal impact that losses will have on the power-electronic devices. This will effect the cooling system requirements and switch lifetime. Therefore, the amount of power lost in each switch is a crucial consideration. Although the cascaded H-bridge inverter improved overall efficiency and reduced overall losses, it actually experienced greater losses per switch than did the full-bridge inverter. Table 5.1 shows the losses experienced in each switch (this table assumes all losses in the H-bridge are spread evenly among switches, since all H-bridge modules will be assigned to each level over its operation). By averaging the data presented in Table 5.1, it can be concluded that each switch in a cascaded H-bridge will dissipate an average of approximately 11% more power than it would in a full-bridge inverter.

**Table 5.1** Power lost per switch in each converter

	<u>750</u> kW/Turbine	<u>1250</u> kW/Turbine	<u>1750</u> kW/Turbine	<u>2250</u> kW/Turbine
P Lost Per Switch In H-bridge (W)	7793.3	10117.8	14650.8	18606.7
P Lost Per Switch In Full-bridge (W)	6568.3	10477.3	13328.7	16462.7
H-bridge vs. Full-bridge	1.187	0.966	1.099	1.130

Another crucial consideration in component sizing was the current passed through each switch. While peak currents tended to be dramatically higher in the cascaded H-bridge, rms currents appeared to be almost similar to the full-bridge values (the software used did not provide a method to compute exact rms values). At the lowest commanded power level, the cascaded H-bridge saw a peak of 1,000 A per switch, while the full-bridge saw a peak of 450 A per switch. At the highest power level, these current peaks increased to 1,800 A for the H-bridge and 1,300 A for the full bridge. Therefore, it can be assumed that each switch in the cascaded H-bridge should be sized to handle twice as much peak current as it would in the full-bridge. However, rms current was only slightly increased in the cascaded H-bridge, by no more than 25% over that of the full-bridge (as can be seen in Figures 4.2 through 4.7). While IGBTs have ratings for both peak and rms current, the rms current rating tends to have a larger affect on cost.

Ultimately, the preliminary study performed in this thesis suggests that the cascaded H-bridge inverter would offer some economic advantages when used in wind farms. A primary benefit can be found in its reduced switch count of four switches per turbine, as opposed to the six switches per turbine in the full-bridge. Another promising economic benefit held by the cascaded H-bridge inverter relates to its simpler interface to the utility. The size of inductors required to filter a cascaded H-bridge inverter is on the order of 10 times smaller than those required for the full-bridge. While their current handling ratings would be dramatically increased, their total count would also be dramatically increased, as only one filter would be required for the entire wind farm (as opposed to the full-bridge system that would require a filter for each wind turbine). Also encouraging is the fact that the cascaded H-bridge inverter can potentially eliminate the

need for a transformer at the point of common connection (depending on what voltage level the power grid to which it connects is operated at). Dramatically increased peak current ratings per switch and slightly increased thermal demands (from power losses) per switch showed the primary drawbacks to the cascaded H-bridge. Power lost per switch in the cascaded H-bridge only increased by around 11% over the full-bridge, and rms collector current increased around 15 to 25% in the cascaded H-bridge. These increases are not large enough to increase the required switch and thermal handling system ratings enough to offset the economic benefit of the cascaded H-bridge. The simulations performed in this thesis also demonstrated that a cascaded H-bridge could be controlled in a stable manner during dynamic wind and power production conditions.

## **5.2 Future Work**

The most important area of future work on this thesis would involve implementing the controller through software code, as opposed to digital logic. While digital logic performed the basic functions that were required for this thesis, any further study or implementation of this concept would require safety override capabilities and advanced switching and control schemes that could only be implemented if the control was implemented in software code (such as C++).

Further study or implementation of this concept would require consideration of other switching and control schemes. Many of these schemes could add more advanced fault recovery control over the H-bridge. Some of these schemes involve the ability to selectively eliminate harmonics, such as paper [16] proposed. Space vector PWM should also be studied. As proposed in paper [11], this method can incorporate advanced fault

recovery methods that take advantage of line to line redundancies (therefore, study of this method would require a cascaded H-bridge model with all three phases). Control methods will need to be simulated that take into account the loss of multiple H-bridge modules (wind turbines). This advanced fault recovery is important because the cascaded H-bridge builds its outputs from the sum of its H-bridge modules, so it is fundamentally less fault tolerant than the full-bridge topology, in which each turbine outputs its power onto the power grid in parallel to one another.

Another potential switching scheme involves adopting an arrangement in which each turbine, or Separate DC Source (SDCS), was given differing voltage levels. As stated in the Introduction, if SDCSs are assigned voltage levels increasing by a factor of two ( $V_{dc}$ ,  $2V_{dc}$ ,  $4V_{dc}$ ,  $8V_{dc}$ ,...), then significantly more voltage levels can be attained, further reducing filtering requirements. This switching method will most likely involve a different amount of switching events per H-bridge module per line cycle (more if a PWM based method is used, perhaps less if a staircase based method is used), so a study of this method would require a reevaluation of the cascaded H-bridge converter's efficiency.

Another important area of future study would involve using the cascaded H-bridge for reactive power support. Since reactive power support would be accomplished through raising or lowering the inverter voltage relative to that of the utility, this would require either raising or lowering the SDCS voltages or altering the amplitude modulation index of the converter. As stated in paper [12], controlling direct-drive synchronous wind farms (cascaded H-bridge wind farms would fall into that category) for reactive power support greatly increases their stability. Thus, the impact that reactive power control would have on efficiency and stability must be studied.

The results that were attained through this thesis indicated that the use of the cascaded H-bridge inverter holds an advantage over the full-bridge inverter when used in wind farm applications. Future experimentations in areas such as switching schemes, fault recovery, and overall control, along with an in-depth consideration of component cost, will need to be performed before the cascaded H-bridge multilevel inverter topology can be either fully adopted or discarded in the domain of wind farm applications.

## **BIBLIOGRAPHY**

- [1] P. Fairley, "Steady As She Blows" *IEEE Spectrum*, August 2003, pp 35-39.
- [2] J. Sloopweg, W. Kling, "Is the Answer Blowing in the Wind?" *IEEE Power And Energy Magazine*, Fall 2002, pp 26-33.
- [3] S. Song, S. Kang, N. Hahm, "Implementation of Grid Connected AC-DC-AC Power Converter for Variable Speed Wind Energy Conversion System," *Applied Power Electronics Conference and Exposition*, Volume 1, 9-13 Feb. 2003 pp 154 - 158
- [4] L. M. Tolbert, ECE 599 Class Notes, The University of Tennessee, Spring 2005.
- [5] L. M. Tolbert, J. N. Chiasson, F. Z. Peng, "Modulation Index Regulation of a Multilevel Inverter for Static Var Compensation," *IEEE Power Engineering Society General Meeting*, Volume 1, 13-17 July 2003
- [6] I. Schiemenz, M. Stiebler, "Control of a Permanent Magnet Synchronous Generator Used in a Variable Speed Wind Energy Conversion System," *International Electric Machines and Drives Conference*, June 2001
- [7] G. Poddar, A. Joseph, A. Unnikrishnan, "Sensorless Variable-Speed Controller for Existing Fixed-Speed Wind Power Generator With Unity-Power-Factor Operation," *IEEE Transactions on Industrial Electronics*, Volume 50, Issue 5, Oct. 2003 pp 1007 – 1015
- [8] L. M. Tolbert, ECE 692 Class Notes, The University of Tennessee, Fall 2004.
- [9] F. Z. Peng, J. W. McKeever, D. J. Adams, "A Power Line Conditioner Using Cascade Multilevel Inverters for Distribution Systems," *IEEE Transactions on Industry Applications*, Volume 34, Issue 6, Nov.-Dec. 1998 pp 1293 - 1298
- [10] M. A. B. Amora, U. H. Bezerra, "Assessment of the Effects of Wind Farms Connected in a Power System," *2001 IEEE Power Tech Proceedings*, Volume 4, 10-13 Sept. 2001 pp 6
- [11] S. Wei, B. Wu, F. Li, X. Sun, "Control Method for Cascaded H-bridge Multilevel Inverter With Faulty Power Cells," *Applied Power Electronics Conference and Exposition*, Volume 1, 9-13 Feb. 2003 pp 261 - 267
- [12] Z. Chen, E. Spooner, "Grid Power Quality with Variable Speed Wind Turbines," *IEEE Transactions on Energy Conversion*, Volume 16, Issue 2, June 2001 pp 148 – 154

- [13] J. Zhang, Y. Zou, X. Zhang, K. Ding, "Study on a Modified Cascade Inverter with Hybrid Modulation," *Proceedings, 2001 4th IEEE International Conference on Power Electronics and Drive Systems*, Volume 1, 22-25 Oct. 2001 pp 379 - 383
- [14] L. M. Tolbert, F. Z. Peng, T. G. Habetler, "Multilevel PWM Methods at Low Modulation Indices," *IEEE Transactions on Power Electronics*, Volume 15, Issue 4, July 2000 pp 719 - 725
- [15] H. K. Al-Hadidi, R. W. Menzies, "Investigation of a Cascade Multilevel Inverter as an STATCOM," *Power Engineering Society General Meeting*, Volume 1, 13-17 July 2003
- [16] J. N. Chiasson, L. M. Tolbert, K. J. McKenzie, Z. Du, "Control of a Multilevel Converter Using Resultant Theory," *IEEE Transactions on Control Systems Technology*, Volume 11, Issue 3, May 2003 pp 345 – 354
- [17] B. Ozpineci, L. M. Tolbert, S. K. Islam, M. Hasanuzzaman, "Effects of Silicon Carbide (SiC) Power Devices on HEV PWM Inverter Losses," *The 27th Annual Conference of the IEEE Industrial Electronics Society*, Volume 2, 29 Nov.-2 Dec. 2001 pp 1061 - 1066

## **Vita**

Gerald Robert (Gerry) Callison was born in Saginaw, Michigan in 1979. He graduated with his B.S.E.E. from the University of Wisconsin- Milwaukee in 2004, and with his M.S.E.E. from the University of Tennessee in 2006. During his graduate studies, he interned in the Power Electronics and Electric Machinery Research Group at Oak Ridge National Laboratory, where he worked with finite element analysis of permanent magnet motors for traction applications. Upon completion of his graduation, Gerry will begin employment at P&H Mining Equipment in Milwaukee, Wisconsin.